EES Catalysis

REVIEW ARTICLE

View Article Online
View Journal | View Issue

Cite this: *EES Catal.*, 2023, 1, 333

Advances in organic semiconductors for photocatalytic hydrogen evolution reaction

Yan Guo, [ab] Qixin Zhou, [a] Bowen Zhu,[c] Chuyang Y. Tang *[b] and Yongfa Zhu *[a]

Received 28th February 2023,
Accepted 17th April 2023

DOI: 10.1039/d3ey00047h

rsc.li/eescatalysis

Using semiconductor materials for solar-driven hydrogen production is a sustainable alternative to fossil fuels. Organic photocatalysts, composed of elements abundantly available on earth, offer the advantage over their inorganic counterparts due to their capacity for electronic property modulation through molecular engineering. However, our understanding of the critical properties of their photocatalytic redox processes has yet to keep pace, hindering further development toward a cost-competitive technology. Here, we expound upon our present comprehension of the microscopic mechanisms underlying organic semiconductor photocatalysis. This article provides an overview of the current state of organic photocatalyst hydrogen evolution reaction (HER), beginning with a description of the charge transfer model of organic semiconductors. We then analyze the excitonic behavior after photoexcitation and present various control strategies aimed at enhancing the efficiency of organic semiconductor photocatalytic hydrogen production. Additionally, we summarize the research progress of conjugated supramolecular and polymeric organic photocatalysts. Finally, we evaluate the efficiency and stability of organic photocatalyst HER.

Broader context

Using semiconductor materials to produce hydrogen from water driven by solar energy is a sustainable alternative to fossil fuels. The origin of this research can be traced back to 1972 when Fujishima and Honda reported the photoelectrochemical hydrogen production catalyzed by titanium dioxide. Despite more than five decades of development, photocatalytic materials have advanced considerably in distinct aspects. However, the precise mechanism underlying photocatalytic hydrogen production, irrespective of whether the catalyst is organic or inorganic, remains incompletely understood. The widely accepted physical model proposes that light generates electron–hole pairs, which then undergo separation and transfer. This mechanism is comparatively intricate for organic photocatalysts in contrast to inorganic ones due to the high exciton binding energy and the inadequately defined migration and transport of electron–hole pairs or free carriers in organic semiconductors. In this review, we present recent research in our group on organic photocatalysts and the findings from previously reported literature. We provide paradigms for future photophysical mechanisms in organic semiconductors and discuss challenges, which we believe will offer valuable insights to researchers exploring photocatalytic hydrogen production.

[a] *Department of Chemistry, Tsinghua University, Beijing, 100084, China. E-mail: Zhuyf@tsinghua.edu.cn*
[b] *Department of Civil Engineering, The University of Hong Kong, Hong Kong, 999077, China. E-mail: tangc@hku.hk*
[c] *School of Environmental and Energy Engineering, Beijing University of Civil Engineering and Architecture, Beijing, 100044, China*

Yan Guo

Dr Yan Guo received her PhD from the Harbin Institute of Technology in July 2022. She is currently a postdoctoral fellow in the Department of Civil Engineering at The University of Hong Kong. Her research focuses on environmental and energy photocatalysis.

Qixin Zhou

Qixin Zhou is a PhD student in the Department of Chemistry at Tsinghua University under the supervision of Professor Yongfa Zhu. His research area is environmental and energy catalysis.

1. Introduction

Photocatalytic water splitting for hydrogen production has emerged as a crucial area of research interest.[1,2] This technology employs solar energy to directly convert water into hydrogen and is thus an important source of clean energy. The development of new photocatalytic materials is critical for achieving efficient water splitting for hydrogen production, given the rapid progress in materials science, physics, chemistry, and related fields. Organic semiconductors are a type of semiconductor that consists of organic compounds such as carbon, hydrogen, oxygen, and nitrogen. Organic semiconductors offer excellent structural tunability, which can be used to adjust their absorption spectra and photoelectric properties to enhance photocatalytic hydrogen production efficiency.[3–5] Moreover, organic semiconductors exhibit greater processability due to their inherent flexibility.[6,7] Inorganic semiconductors continue to be the most commonly used photocatalysts in the study of photocatalytic water splitting for hydrogen production,[8,9] owing to their advantages such as higher photoelectric conversion efficiency and better stability.[10,11] For instance, the external quantum efficiency of aluminum-doped $SrTiO_3$ at the ultraviolet wavelength (350–360 nm) is 96%.[12] However, given that less than 5% of solar energy falls within the ultraviolet spectrum, visible-light-active photocatalysts are needed to achieve the 5–10% solar-to-hydrogen conversion efficiency (ηSTH) necessary for commercial viability. This has led to recent interest in the development of organic semiconductor-based photocatalysts.[3,14] Although the hydrogen production rates (HER) of organic photocatalysts based on half-reactions are now comparable to those of inorganic photocatalysts, the low rate of overall water splitting (OWS) and their stability remain a challenge.

The photocatalytic mechanism for hydrogen production using both organic and inorganic photocatalysts is not yet fully understood, and the widely accepted physical model involves processes such as the separation and transfer of photogenerated electron–hole pairs, reduction of photogenerated electrons on the surface of the catalyst, and oxidation of photogenerated holes on the surface. The migration and transport of electron–hole pairs/free carriers in organic semiconductors are not clear due to the high dissociation energy of excitons and molecular crystal properties, making the exploration of the photocatalytic mechanism for hydrogen production more complex for organic photocatalysts.[13] Currently, there is no literature that examines the influence of the electronic structure and exciton behavior of organic semiconductors on photocatalytic HER. Therefore, based on our group's research on organic photocatalysts and the reported results, we have written this review to provide inspiration to researchers studying photocatalytic hydrogen production. We first outline the current status of organic photocatalyst HER, highlighting the charge transfer model of

Bowen Zhu

Bowen Zhu is an undergraduate student in the School of Environmental and Energy Engineering at Beijing University of Civil Engineering and Architecture. His research interests are in environmental and energy photocatalysis.

Chuyang Y. Tang

C. Y. Tang is a Professor of Environmental Engineering at the University of Hong Kong and leads the Membrane-based Environmental & Sustainable Technology (MemBEST) group. He received his BE (First Class Honors, 2000) and ME (2001) degrees from Nanyang Technological University and his PhD degree (2007) from Stanford University. Professor Tang's research focuses on membrane and filter technology, environmental materials, desalination, water reuse, resource recovery, and water-energy nexus. He has over 300 refereed publications, with a total citation of >35 000 and H-index of 103 (Google Scholar). He has been recognized as a Clarivate Highly Cited Researcher since 2021.

Yongfa Zhu

Yongfa Zhu is a professor in the Department of Chemistry, Tsinghua University, and the Executive Deputy Director of the National Center for Electron Spectroscopy. He received BS, MS and PhD degrees from Nanjing University, Peking University and Tsinghua University, respectively. He has been researching energy, environmental, and health photocatalysis at Tsinghua since 1988. He has received funding from Trans-Century Training Programme Foundation for the Talents by the State Education Commission and the National Natural Science Fund for Distinguished Young Scholars. He has been recognized as a Elsevier Highly Cited Scholar since 2014 and as a Clarivate Highly Cited Researcher since 2018. He ranked 851st among the Top 100 000 Scientists globally in 2021.

organic semiconductors; then analyze the excitonic behavior after photoexcitation; provide control strategies to enhance the efficiency of organic semiconductor photocatalytic hydrogen production; summarize the research progress of conjugated supramolecular and polymeric organic photocatalysts; and finally, evaluate the efficiency and stability of organic photocatalyst HER.

2. Status of photocatalytic HER in organic semiconductor

Photocatalytic hydrogen evolution reaction (HER) from water requires a semiconductor photocatalyst with a bandgap energy that is at least as high as the electrochemical potential needed to drive the overall water splitting (OWS). Practical photocatalysts should have a bandgap of 1.8 to 2.0 eV to accommodate the overpotential required for observable reaction rates for both HER and oxygen evolution reaction (OER). Suitable photocatalysts for OWS are attractive and challenging. Currently, there is controversy in HER regarding sacrificial donors and co-catalysts. Additionally, the potential for scalable applications is also gaining attention.

2.1 Requirement of sacrificial donors

Water splitting to produce hydrogen is challenging due to the four-electron reaction required for O_2 evolution from water ($O_2(g) + 4H^+(aq) + 4e^- \rightarrow 2H_2O$ (l), E = +0.82 V *vs.* SHE at pH 7). This has led to the use of sacrificial donors such as triethylamine (TEA), which is thermodynamically less demanding than water and has a two-electron reaction (diethylamine (aq) + acetaldehyde (aq) + $2H^+$ (aq) + $2e^- \rightarrow$ triethylamine (aq) + H_2O(l), E = −0.72 V *vs.* SHE at pH 11.5, pH of triethylamine solution), making it kinetically faster. The challenges and limited success in OWS have prompted researchers to use sacrificial agents to separate HER from water oxidation to independently study the two half-reactions. Common sacrificial donors used in HER include methanol, triethylamine, ascorbic acid, triethanolamine, and EDTA. Photocatalytic reactions consume sacrificial donors, necessitating continuous addition to maintain H_2 production. Whether the source of hydrogen in HER is water or a sacrificial donor has been called for and requires evidence to clarify.[14,15] Because these sacrificial donors are rich in carbon and hydrogen, the oxidation of methanol, for example, produces C1 products and hydrogen. The role of sacrificial donors has been reviewed in detail.[16] Currently, organic photocatalysts for the OWS without sacrificial donors are attractive but difficult to design.[17,18] One approach being the deposition of HER and OER co-catalysts, where the distribution of the two co-catalysts is critical. Another approach is to construct a Z schemes, whose complex device design and higher cost make it less attractive than a single-step system, and where charge transfer requires overcoming additional processes related to the interface between the two materials.

2.2 Requirement of co-catalysts in organic photocatalysts

Photocatalytic water splitting differs from electrocatalytic water splitting in that it relies on photogenerated carriers to drive the associated redox reactions, whereas electrocatalytic water splitting depends on an external potential to supply the charge and driving force. Despite differences in the generation and transport of charges to active sites, both electrocatalytic and photocatalytic systems share a localized electrochemical process for reactant-to-product conversion. The use of metal co-catalysts with electrocatalytic properties is often necessary to provide active sites for photocatalysts,[19,20] and noble metals have become the preferred choice due to their exceptional catalytic properties, despite their high cost and scarcity. To reduce the loading of noble metals in organic photocatalysts while maintaining performance, several approaches, including single-atom catalysis, bimetallic co-catalysts, and the exploration of metal-free photocatalytic systems, can be used to optimize resource utilization and achieve a balance between the crucial role of co-catalysts and the need for environmental sustainability in photocatalysis.

2.2.1 Atomically dispersed metal centers. The utilization of atomically dispersed metal centers has been investigated in the synthesis of single-atom photocatalysts for H_2 evolution on two-dimensional PCN, a commonly used organic semiconductor. The abundant surface trapping sites for isolated atoms on PCN make it an excellent host support. Various types of isolated metal sites, including noble and non-noble metals (*e.g.*, Pt,[21–23] Pd,[24,25] Rh,[26] Au,[27] and Ag[28]) and non-noble metal (*e.g.*, Fe,[29] Co,[30] Ni,[31] Cu,[32] and Ga[33]), have been decorated on PCN to significantly lower the energy barrier for H2 evolution and reduce the metal loading. However, the achievement of uniform dispersion of isolated reaction centers on semiconductor supports requires sufficient distances between each metal precursor to prevent agglomeration and ensure the formation of single-atom photocatalysts with specific geometric environments after post-processing. These strict requirements on the support limit the widespread application of single-atom co-catalysts to a certain extent.

2.2.2 Bimetallic co-catalysts. Bimetallic nanoparticles have been found to improve the intrinsic activity of cocatalysts and reduce loading capacity. They do so by regulating the separation and migration kinetics of interfacial photogenerated carriers and providing abundant surface-active sites. The band hybridization between the two metals and the charge redistribution within the bimetal also enhance the charge separation efficiency. Furthermore, bimetallic nanoparticles offer numerous catalytic active sites for surface reactions, which regulate the adsorption and activation behavior of reactants and target products on the catalyst surface. This improves the activity and selectivity of photocatalytic reactions. Benefiting from the intrinsic properties and delicate design of bimetallic NPs, the specific activity of organic semiconductor/bimetallic NPs-based catalysts is significantly better than that of monometallic catalysts (*e.g.*, Pt/Au,[34,35] AuPd,[36] PtCo,[37] FeCu,[38] NiCu,[39] NiMn[40]).

2.2.3 Entirely metal-free photocatalytic systems. In pursuit of green and sustainable chemistry, the exploration of efficient and stable entirely metal-free photocatalysts for water photoreduction to H_2 remains a formidable challenge. One potential approach involves utilizing metal-free co-catalysts (*e.g.*, Carbon Dots,[41] Black Phosphorous[42]), which entirely circumvent the introduction of metal elements. Moreover, recent reports have shown that the synthesis of these polymers or precursors was carried out *via* metal catalysts,[43,44] which may leave residual metal and have the potential to act as a co-catalyst. This highlights the importance of developing metal-free synthetic routes for these co-catalysts.

2.3 Scalable application

The application of the particle suspension process to industrial production presents challenges such as power consumption for powder dispersion and powder separation from the suspension. Therefore, the immobilization of photocatalyst powder onto a specific substrate is necessary to scale up photocatalytic HER from laboratory to plant scale. Although a solar-to-hydrogen (STH) efficiency of 5–10% is required for economically viable solar hydrogen production, few reports have achieved STH of almost 10%. However, as mass transfer in immobilization is less effective than in the suspension industry, further studies on immobilized photocatalyst systems are necessary for future applications. For inorganic photocatalytic HER, aluminum-doped strontium titanate has been reported with an STH of 0.76% in a 100 m^2 plate reactor array. The devices are made by depositing aluminum-doped strontium titanate onto frosted glass *via* a programmed spray system with the addition of hydrophilic silica particles to form mesoporous channels in the inter-particle voids and facilitate water and gas transfer. InGaN/GaN NWs supported on silicon wafers were synthesized by molecular beam epitaxy, achieving an STH of 9.2% at 70 °C[1]. Organic semiconductors can be prepared as flexible devices by forming thin films on flexible substrates using solution processing techniques without requiring high temperatures, vacuum or atmospheric conditions. This allows for a wide range of applications in large area and mass production. Flexible devices have been prepared by cementing PTA onto cellulose nonwovens *via* hydrogen bonding.[45] In our recent study, hydrogen-bonded organic frameworks have also been prepared into flexible devices through hydrogen bonding for scalable photocatalytic HER. Other mechanically strong substrates should be considered to obtain more stable flexible devices.

3. Charge carrier transfer and photoexcited electron processes in organic semiconductors

During the process of photocatalytic HER, organic semiconductors absorb light energy and generate electron–hole pairs (A neutral exciton since Coulomb interaction is strong). These excitons can migrate and diffuse to the semiconductor surface, where they combine with protons in water to form hydrogen

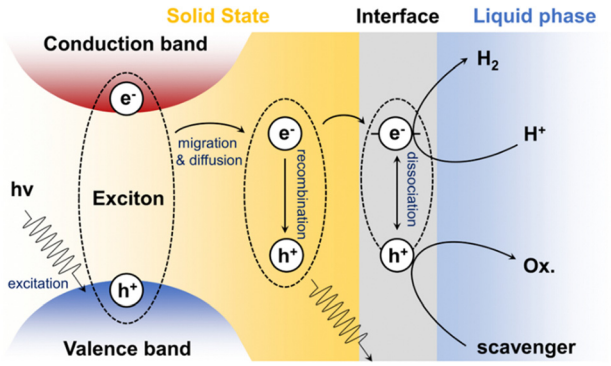

Fig. 1 Schematic diagram of organic semiconductor photocatalytic HER.

(as shown in Fig. 1). The structure of the organic semiconductor is critical in the generation and diffusion of photoinduced excitons.

3.1 Charge carrier transport in organic semiconductors

The highly ordered structure and minimal defects of crystals provide a prerequisite for revealing the mechanism of charge transport. In organic semiconductors, the carrier transport model is complex due to non-covalent interactions between adjacent molecules.[46] Few studies have explored the transport of charge carriers in organic semiconductors in the field of photocatalysis, with most only evaluating the efficiency of charge carrier transport based on charge separation results. Several theories for evaluating the charge carrier transport mechanism in organic semiconductors exist in the field of semiconductor physics, including band-like transport, small polaron hopping, multiple trapping and releasing models, and their modifications.[47] Organic photocatalysts often have a conjugated aromatic ring structure, enabling good light absorption and excitation capabilities and facilitating electron transport in molecular materials.[48] The transport of excitons is often realized through a band-like transport mode in the photochemical reaction process of reported organic photocatalysts.[49] This mode involves the transport of excitons formed by the transition of electrons between molecular energy levels within the molecular material. The conjugated structure within the molecular material enables electrons to move inside the molecule and transition between adjacent molecular energy levels. Understanding how the electrons and holes generated in organic semiconductors after photoexcitation are transported within the material can help researchers comprehend the rate and efficiency of catalytic reactions and guide the design of new materials.[50]

3.2 Generation of excitons

When light energy exceeds the optical bandgap of the organic material, photons are absorbed by the molecule, causing a transition from the ground state to the excited state. Electrons in the molecule transition from the HOMO to the LUMO or higher energy levels, forming excitons or bound electron–hole pairs within the molecule. Excitons can be classified into three

categories based on the distance between the electron–hole pair: Frenkel excitons, CT excitons, and Wannier excitons. Frenkel excitons, with the smallest radii and average electron–hole distances within a lattice constant of about 5 Å, indicate that electrons and holes are confined to the same molecule and possess strong Coulomb binding energies of about 0.3–1.0 eV. Wannier excitons have an exciton radius of about 40–100 Å and a much lower binding energy than Frenkel excitons, at approximately 0.01 eV. The presence of Frenkel excitons is observed in organic systems due to their low dielectric constant, whereas Wannier excitons are typically present in inorganic systems.[51] CT excitons have an exciton radius between that of Frenkel and Wannier excitons, within one or two lattice constants. After exciton formation, they may diffuse or evolve, dissociate into electron–hole pairs, merge into a single exciton, split into two excitons, be trapped or localized, and ultimately annihilate or emit.[52] To achieve efficient photocatalytic processes, enhancing photon absorption, extending the exciton diffusion length and effective dissociation, rapid transport of electron–hole pairs, and minimizing electron–hole pair recombination are crucial.

3.3 Migration and diffusion of exciton

Organic semiconducting materials with high exciton migration rates and diffusion lengths are beneficial for enhancing photocatalytic HER.[52,53] Exciton migration and diffusion rates determine the transport efficiency of photogenerated electrons and holes within the material. Faster exciton migration rates allow for easier movement of charge carriers within the material, enhancing hydrogen production performance. Conversely, slow exciton migration rates result in charge carrier recombination within the material, leading to reduced hydrogen production efficiency. Excitons have a finite lifetime and move within a solid, interacting with other excitons, molecules, or lattice defects.[54] The exciton diffusion length is the average distance that an exciton moves from its initial position within its lifetime and is related to the exciton's lifetime, the material's lattice structure, and its optical properties.

The diffusion coefficient D is used to measure the diffusion ability of excitons, which is related to the exciton diffusion length L and lifetime t in space and time, respectively. For homogenous diffusion, the exciton diffusion length is described by eqn (1):[55]

$$L = \sqrt{ZD\tau} \quad (1)$$

where τ is the exciton lifetime, D is the diffusion coefficient, and Z is equal to 1, 2, or 3 for one-dimensional, two-dimensional, or three-dimensional diffusion, respectively.

Only charge carriers that successfully reach the surface of the photocatalyst can participate in the photocatalytic hydrogen production process. The mobility of organic semiconductors can be enhanced by improving their crystallinity.[56]

3.4 Dissociation of excitons

Excitons in organic semiconductors do not spontaneously dissociate into free electron–hole pairs due to their relatively high binding energy. However, exciton dissociation can occur at the interface between electron/hole acceptors, and strong electric fields can also assist the separation process.[55,57] For example, fullerenes have a lower LUMO than many organic semiconductors, promoting electron transfer and exciton dissociation. Fullerenes can dissociate excitons within 45 fs, much shorter than the typical exciton lifetime ($\sim$0.5 ns), making them efficient quenchers.[58–60] Exciton density, PL intensity, and PL decay time are characteristics used to measure exciton dissociation. Choosing the appropriate exciton dissociation method is necessary to optimize photocatalytic performance of specific organic photocatalysts or device structures, and adding a sacrificial agent donor can promote exciton dissociation.

3.5 Proton reduction from water

Based on the dissociation of excitons, photogenerated electrons are typically involved in two scenarios for reducing protons in hydrogen production. In one scenario, the undissociated exciton reaches the interface between the photocatalyst and water. The hole in the exciton is captured by the absorbed H_2O/sacrificial donor, while the electron is separated and used to reduce the reductive adsorbed proton.[61] Alternatively, the excitons are separated into electrons and holes in the bulk of photocatalyst. The electrons then arrive at the surface and reduce the adsorbed protons. In half-reaction hydrogen production from organic photocatalysts, it is essential to determine the source of protons, whether from the catalyst,[15] water, or the sacrificial donor, which can be accomplished by analyzing the reaction products. Furthermore, detecting the proton source requires the use of D_2O instead of H_2O. In addition to the aforementioned factors, pH is also a critical determinant of the origin of hydrogen protons. In acidic conditions, the concentration of protons in water is high, and water serves as the primary source of hydrogen protons. Conversely, under alkaline conditions, the concentration of hydrogen ions in water is low, and sacrificial donors become the primary source of hydrogen protons. Probing the source of hydrogen protons allows a better understanding of the photocatalytic HER mechanism and enable the optimization of HER conditions.

4. Strategies for enhancing the photocatalytic HER in organic semiconductor

The great advantage of organic semiconductors lies in the structure tunability. Compared to inorganic photocatalysts, it is easy to enhance the photocatalytic efficiency by modulating chemical and crystal structures. To improve the efficiency of photocatalytic HER, effective strategies include expanding the light absorption range, tuning appropriate reduction ability, dissociating more excitons, exposing more active sites and optimizing exciton behavior (Fig. 2).

4.1 Light absorption range

Conjugated structure pertains to the uninterrupted π-electron system in organic molecules. Extending the conjugated structure

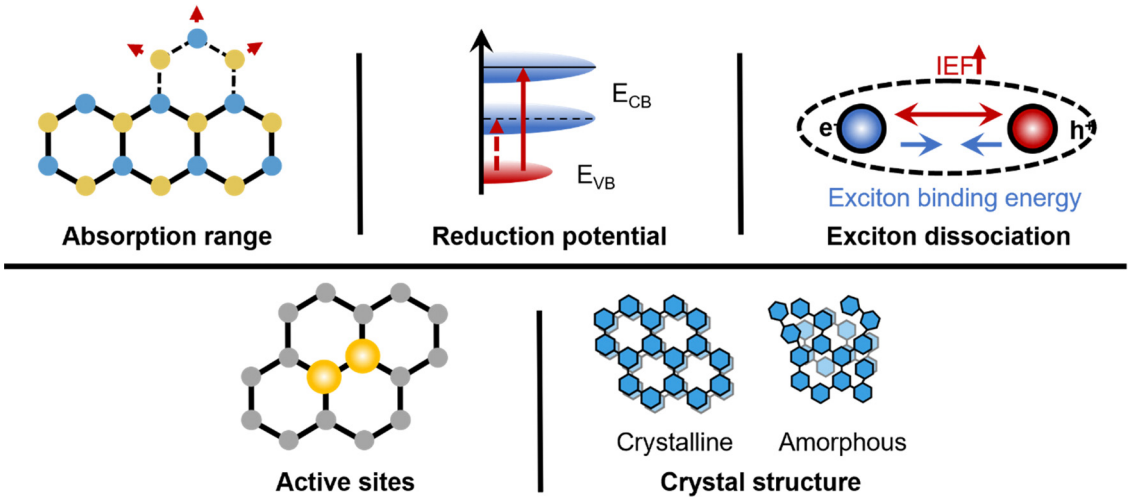

Fig. 2 Strategies for enhancing the photocatalytic HER of organic semiconductor.

by introducing aromatic, nitrogen-containing, oxygen-containing, or sulfur-containing heteroatoms can broaden the light absorption range of organic photocatalysts.[62–64] These heteroatoms alter the distribution of π-electrons in the molecule, augment the size and complexity of the conjugated system, and amplify the molecular absorption spectrum range. Furthermore, controlling the arrangement of the conjugated system can modulate the optical properties of organic molecules. For instance, altering the position and orientation of double bonds can regulate the length and shape of the conjugated system, thereby modifying the absorption spectrum range and optical properties of organic molecules.

4.2 Redox capacity

The redox ability of a photocatalyst during photocatalytic HER is determined by its conduction band position, which is influenced by the molecular structure, specifically functional groups and conjugated structures within the molecule.[65] A higher reduction potential is favorable for overcoming the overpotential in the HER process. However, increasing the reduction potential may widen the band gap, leading to a narrower absorption range. By introducing electron-donating or electron-withdrawing functional groups and conjugated structures, the conduction band position of organic photocatalysts can be controlled.[66] For example, adding elements such as nitrogen, oxygen, and sulfur to organic molecules modifies their electron affinity and transport properties, thereby affecting the conduction band position. In addition, changes in the spatial position of the molecular functional groups affect the electron conjugation, which can be monitored by calculating the electron cloud in the π orbitals.

4.3 Exciton dissociation

Electrons involved in photocatalytic hydrogen production *via* water reduction originate from exciton dissociation. Frenkel excitons in organic molecular crystals generally possess binding energies exceeding room temperature thermal energy,[67] impeding the spontaneous dissociation of photogenerated excitons into unbound charge carriers 51. Moreover, the exciton diffusion length in organic crystals is shorter than in inorganic counterparts, complicating exciton separation. To facilitate exciton dissociation, an exciton confinement region can be established by creating a proximal interface, subsequently diminishing electron–hole pair migration distances. Additionally, modulating internal electric fields (IEFs) has proven effective in dissociating organic excitons.[68,69] To dissociate excitons into unbound charge carriers, the IEF strength must surpass exciton binding energy.

$$r_B \times e \times F_{IEF} \geq E_B \quad (2)$$

Here, r_B is the Bohr radius of the exciton (nm), e is the electronic charge, F_{IEF} is the strength of the IEF within the photocatalyst (mV nm^{-1}), and E_B is the binding energy of excitons (meV). The testing methods for the strength of the IEF have been summarized in the literature, and the binding energy of excitons can also be obtained by fitting variable-temperature fluorescence emission data.

Utilizing eqn (2), the adequacy of IEF strength for exciton dissociation into unbound charge carriers can be determined. Consequently, organic photocatalyst design necessitates consideration of both IEF strength and interface structures to facilitate Frenkel exciton dissociation and augment photocatalyst efficiency. In recent years, materials including porous and 2D substances have demonstrated potential in diminishing exciton migration distances from bulk to dissociation interface, thereby promoting exciton dissociation. These discoveries offer valuable insights for designing and optimizing organic photocatalysts.

4.4 Active aites for HER

Photocatalytic water splitting efficiency and hydrogen production selectivity are contingent on catalyst active sites.[70–72] Active sites/regions for hydrogen production include adsorption of *H sites, –H-containing functional groups, and photogenerated electron-rich areas. The diiron [Fe_2S_2] subunit operates as the

proton reduction catalytic center, with the $[Fe_4S_4]$ cluster facilitating electron transfer to and from the H-cluster active site.[73] Incorporating functional groups like oxides and nitrides onto transition metal surfaces can enhance *H site adsorption. Moreover, constructing donor–acceptor structures and separating electrons and holes can generate photo-induced electron-rich regions.[74] Regulating active site local electronic structures can also improve hydrogen production efficiency. For example, forming a Pt–I_3 site on a photocatalyst surface results in a potent metal-carrier interaction, yielding hydrogen production performance approximately 176.5 times greater than that of Pt nanoparticles on the photocatalyst.[75] Implementing these regulatory approaches necessitates a comprehensive understanding of photocatalyst electronic structures and catalytic reaction mechanisms, drawing from interdisciplinary knowledge in chemistry and physics.

4.5 Crystal structure

The exciton behavior and surface reactions in organic semiconductors are influenced by crystallinity, molecular stacking mode, and morphology, subsequently impacting the hydrogen evolution reaction (HER) performance of organic photocatalysts.[76,77] Highly crystalline materials generally facilitate carrier migration while ameliorating surface and structural defects,[78] diminishing free carrier quenching, and augmenting catalyst active site density. Organic semiconductors exhibit instability under high-energy electron beam irradiation, posing limitations on crystallinity characterization.

Anisotropic molecular arrangements dictate charge carrier migration rates in organic semiconductor materials, enabling regulation of migration rates by controlling molecular stacking modes. Within organic field-effect transistor (OFET) research, π–π stacking is deemed the most effective charge carrier transport method.[79,80] Large π–π overlap (more delocalized states) stabilizes +1 or −1 charged states, fostering polarizable or band-like charge carrier transport and enabling efficient intermolecular charge transfer. Solvent vapor treatment can regulate molecular stacking modes and control π–π stacking formation.

Morphology can modulate the exposure of active sites such as *H, –H, and photo-generated electron-rich regions. Constructing porous structures effectively exposes active sites, with the confinement effect generated by pores being more conducive to hydrogen production.

5. Applications of organic semiconductors in photocatalytic HER

Recently, the investigation of organic semiconductors in photocatalytic hydrogen evolution reaction (HER) research has garnered significant interest, primarily concentrating on two classes of organic semiconductors: conjugated supramolecular systems and polymers. In the context of the former, this review emphasizes the utilization of small molecule aggregates and metal–organic frameworks (MOFs) as organic photocatalysts for HER. For the latter, the potential of covalent organic frameworks (COFs) and polymer carbon nitride (PCN) organic photocatalysts for HER is examined.

5.1 Conjugated supramolecular organic semiconductor photocatalysts

Conjugated organic molecules generally comprise numerous aromatic rings or conjugated double bonds, with their π electrons establishing a conjugated system exhibiting favorable electron conductivity and light absorption.[81] Intermolecular interactions facilitate the formation of stacked structures.[82] The photocatalytic hydrogen production performance is predominantly dictated by the chemical and crystal structures. We emphasize the regulation of exciton behavior and reduction capacity by the chemical structure of conjugated molecules.

5.1.1 Small molecule crystals. Effective exciton dissociation transpires at the interface of electron/hole capture agents, with a robust electric field assisting in exciton separation. Uneven charge distribution within molecules generates molecular dipoles, and orderly stacking amplifies the internal electric field (IEF) within molecular crystals. Altering functional groups in organic molecules can impact their molecular dipoles, enabling effective separation of photogenerated electron–hole pairs through the strategic design of functional groups to regulate dipole fields. Our research group has extensively investigated the dipole field in molecular crystals of a single-molecule-thick Perylenetetracarboxylic acid (PTA) nanosheet photocatalyst.[45]

As depicted in Fig. 3a, PTA molecular electrostatic potential calculations reveal a minimal electrostatic potential on the terephthalic plane, whereas the edge carboxyl groups exhibit a negative potential, creating a local dipole from the terephthalic acid molecule's center to its edge. Conversely, the electrostatic potential of the phthalocyanine derivative (PTCDA) is less distinct. The dipole field direction within the crystal was determined based on the established PTA molecular stacking direction and crystal structure. Additionally, the hydrogen bond polarization of the carboxyl group in PTA can enhance the IEF. As illustrated in Fig. 3b, the ordered crystallinity of PTA contributes to macroscopic IEF accumulation. The IEF direction was verified through Mn_2O_3 and Pt photodeposition (Fig. 3c and d). The charge transfer resistance of PTA, as determined by impedance spectrum fitting, is 36 kΩ, lower than that of PTCDA (21 770 kΩ) (Fig. 3e). The enhanced IEF enables a carrier generation rate of 90.6% for PTA nanosheets, with a 2.9-fold increase in electron migration rate (Fig. 3f), signifying that the enhanced IEF facilitates charge transfer from bulk to surface. The photocatalytic hydrogen evolution rate of PTA reaches an impressive 118.9 mmol g^{-1} h^{-1}.

Porphyrins are large conjugated molecules characterized by an extensive π aromatic ring structure and 18 delocalized electrons. Prior research in photocatalysis has emphasized employing the effective light absorption and electron transfer properties of porphyrins as photosensitizers. Nonetheless, the self-degradation of porphyrin molecules during sensitization has posed a significant challenge. Recently, nano self-assembly has effectively addressed the stability issue, with the formation of self-assembled aggregates enhancing solar absorption and

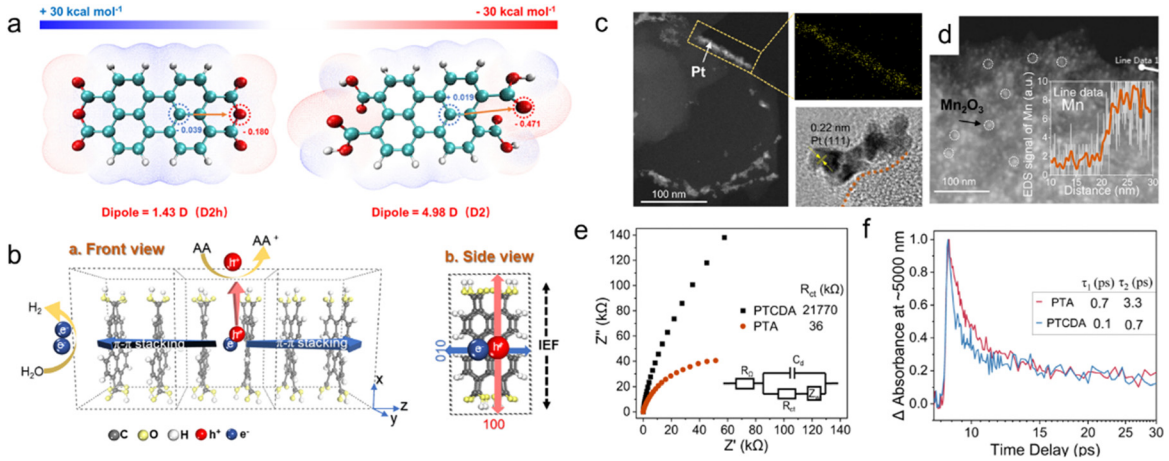

Fig. 3 (a) Molecular dipole calculations. The dipole moment of PTCDA (left) and PTA (right) based molecular electrostatic potential. (b) Schematic diagram of IEF in PTA cell. ADF-STEM photodeposition on PTA with (c) Pt and high resolution and mapping, (d) Mn_2O_3 (inset: Mn element liner scan). (e) impedance and (f) transient absorption decay kinetics at ~5000 nm of PTCDA and PTA. Reproduced with permission from ref. 45 (Copyright 2022, Springer Nature).

improving cycling stability.[83,84] Various porphyrin derivatives arise from attaching different electronegative substituents, such as pyridine, cyanide, and carboxyl groups, to the R position of porphyrin molecules (Fig. 4a). The polarity differences of these groups regulate the dipole moment of the porphyrin molecule.

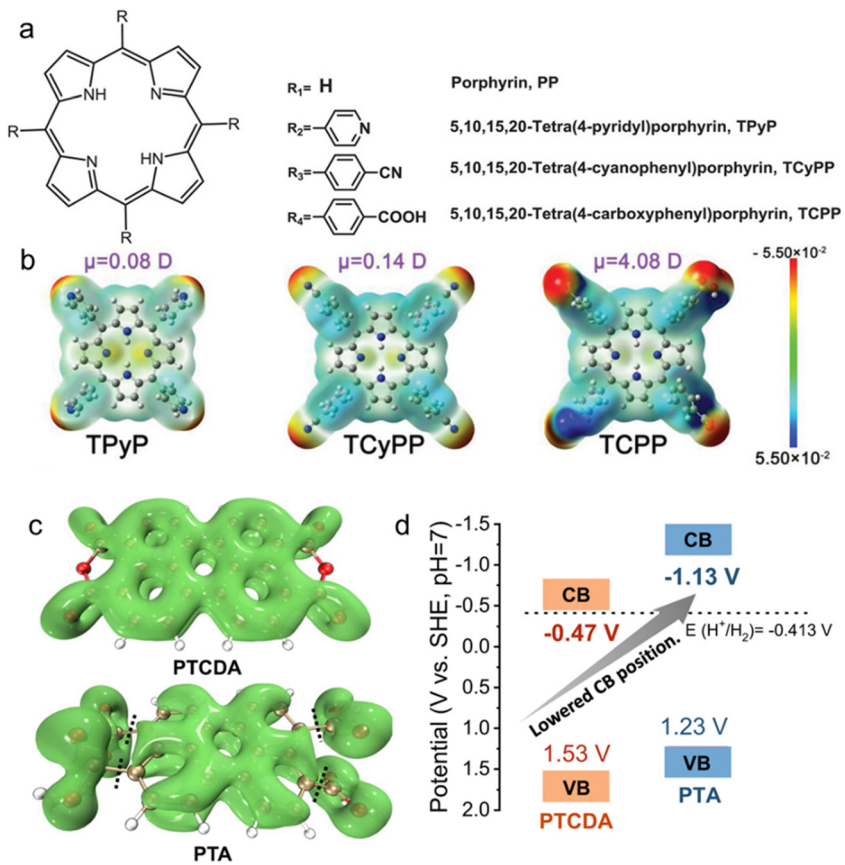

Fig. 4 (a) Molecular structures of several porphyrin derivatives with different dipoles. (b) Diagram of molecular dipoles and electrons distribution in three porphyrin derivatives, unit of dipole moment: Debye. Reproduced with permission from ref. 85 (Copyright 2019, Wiley-VCH). (c) The localized orbital locator-π (LOL-π) isosurface. (d) The band structures of PTCDA and PTA measured experimentally. Reproduced with permission from ref. 45 (Copyright 2022, Springer Nature).

Theoretical calculations suggest that electronegative substituents augment the dipole moment of the porphyrin molecule. As demonstrated in Fig. 4b, employing a carboxyl group as a substituent result in a substantial potential difference between the central and end substituents of the porphyrin ring, with the maximum dipole moment reaching 4.08 Debye. In comparison to the photocurrent of TCPP, approximately 0.1 μA cm^{-2}, the photocurrent of SA-TCPP is as high as 3.52 μA cm^{-2}, signifying that a strong dipole electric field enhances charge separation efficiency. Upon effectively separating the photogenerated electron–hole pairs with a robust dipole electric field, the photogenerated charges are transported along the π–π channel to the surface, allowing TCPP photocatalysts to produce hydrogen and oxygen from water without the assistance of a co-catalyst.[85]

The degeneracy of the isolated molecule LUMO energy level increases, forming degenerate bands in organic crystals. The LUMO energy level of organic molecules is influenced by their electron affinity and electron-withdrawing properties, which are closely related to the molecular structure.[86] Generally, molecules with higher electron affinity and lower electron-withdrawing properties possess lower LUMO energy levels, whereas those with lower electron affinity and higher electron-withdrawing properties exhibit higher LUMO energy levels. Factors such as substituent groups (*e.g.*, oxygen atoms, halogens, and methylene groups), conjugated structures, and molecular shape also impact the LUMO energy level. Conjugated structures can enhance the degree of π-electron conjugation in the molecule, thereby augmenting its electron-withdrawing property and lowering its LUMO energy level. Moreover, molecular shape can affect the distribution of π-electron cloud in the molecule *via* steric hindrance and spatial orientation.

For instance, rotating or twisted bonds in a molecule can hinder the π-electron cloud at these positions,[87] disrupting the conjugation (also known as steric hindrance effect). For a molecule containing a phthalocyanine plane, altering the edge from an anhydride structure (PTCDA) to a carboxylic acid structure (PTA) decreases the molecule's planarity due to the steric hindrance of the carboxylic acid and the twisting of the phthalocyanine plane, resulting in reduced conjugation throughout the entire molecule.[88] The π orbitals in the molecule were measured using a localized orbital locator-π (LOL-π) isosurface. As shown in Fig. 4c, the π orbitals of the PTCDA molecule extend to the entire molecular plane. Conversely, a nodal plane appears on the π orbital of the PTA molecule, where the phthalocyanine plane intersects the carboxyl group. This decrease in molecular conjugation leads to a lower LUMO energy level for PTA, endowing PTA nanosheets with adequate reduction potential for HER (Fig. 4d).

5.1.2 Metal–organic frameworks (MOFs). Metal–organic frameworks (MOFs) are semiconductor materials formed through self-assembly driven by coordination between metal or metal cluster centers and photoactive organic ligands, displaying exceptional potential in photocatalysis due to their excellent structural designability and regular porous structure.[89] The ligand-to-metal charge transfer (LMCT) process is nearly a universal principle in the design of MOF photocatalysts.

Two MOFs, Ti_3-BPDC-Ir and Ti_3-BPDC-Ru, have been reported,[90] which investigates the charge transfer process. Photophysical and electrochemical studies reveal that electrons are transferred from the reducing photosensitizer to $Ti_3(OH)_2$, resulting in photocatalytic hydrogen production with conversion rates of 6632 and 786, respectively. Based on the well-defined catalytic center structure in MOFs, the researchers propose a photocatalytic HER through a Ti^{IV} -hydride intermediate (Fig. 5a and b). The low-coordinate Ti^{III} center accepts a proton from H_2O and an electron from another reducing photosensitizer [Ir(ppy)2(dcbpy)] to form a Ti^{IV}-hydride intermediate, thereby performing proton-coupled electron transfer. Protonation of Ti^{IV} -hydride produces hydrogen gas and regenerates Ti^{IV}-OH catalysts.

Interestingly, another study found that the introduction of different functional groups significantly affects the lifetime of Ti^{3+} intermediates generated during the LMCT process,[91] resulting in significantly different dark state photocatalytic hydrogen production activity (Fig. 5c). The number of Ti^{3+} intermediates generated by MIL-125-NH_2 with electron-donating groups is large and has a long lifetime, exhibiting enhanced activity, while the number of Ti^{3+} intermediates generated by MIL-125-X (X = NO_2, Br) with electron-withdrawing groups is small and has a short lifetime (Fig. 5d), showing reduced activity (Fig. 5e).

The Ag(I) cluster-based nodes can allow efficient LMCT or MLCT/CLCT and help improve photocatalytic performance, while the plasmonic effect of silver-containing materials produces a synergistic effect. For example, Ag-AgMOM has been developed,[92] with the highest occupied valence band (HOVB) rotating upward and located on the AgO_4 junction, while the lowest unoccupied conduction band (LUCB) rotates downward and is distributed in the porphyrin of TCPP (Fig. 5f). The strong interaction between the plasmonic AgNPs and excited AgMOM promotes the photocatalytic HER (Fig. 5g), exhibiting a hydrogen production rate of up to 1025 μmol h^{-1} g^{-1} in visible light photocatalysis and further increasing to 3153 μmol h^{-1} g^{-1} under full-spectrum irradiation (Fig. 5h).

5.2 Conjugated polymer organic semiconductor photocatalysts

5.2.1 Covalent organic frameworks (COF) polymer. Covalent organic frameworks (COFs) are two-dimensional or three-dimensional network materials formed by organic molecules connected by covalent bonds,[93] displaying unique attractiveness in photocatalysis applications due to their tunable structure and pore size.[94] The design and synthesis of COFs, as well as the control of pore structure and confinement effects, have been extensively reviewed.[95–97] In this discussion, we emphasize the degree of conjugation between the linker and monomer, which is one of the critical factors in achieving excellent photocatalytic performance of COFs. Furthermore, we aim to highlight the study of exciton behavior in COFs.

First, the degree of conjugation between the monomer and linker has a significant impact on the optoelectronic properties of COFs.[98] When the π-electron energy levels of the linker and monomer are coupled, a conjugated system is formed, which

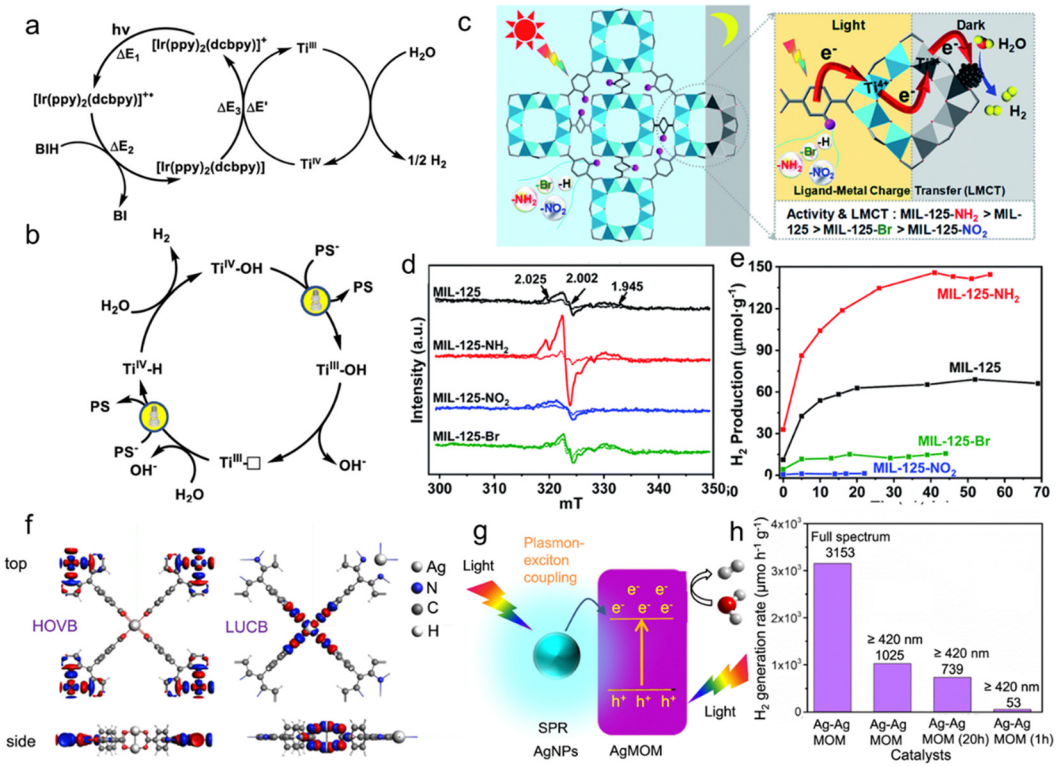

Fig. 5 (a) Proposed Catalytic Cycle for the Visible Light-Driven HER Catalyzed by Ti_3-BPDC-Ir; (b) detailed catalytic mechanism on the Ti Site *via* the Ti^{IV}/Ti^{III} Cycle. Reproduced with permission from ref. 90 (Copyright 2019, American Chemical Society). (c) Illustration showing the dark photocatalysis over MIL-125 and MIL-125 with different functional groups, MIL-125-X (X = NH_2, NO_2, Br). (d) Dark photocatalytic hydrogen production activity comparison of MIL-125 and MIL-125-X (X = NH_2, NO_2, Br) with 0.5 mL TEOA as a sacrificial agent at 25 °C. (e) ESR spectra (solid and dotted lines represent signals in the dark and when light is on, respectively) for MIL-125 and MIL-125-X (X = NH_2, NO_2, Br). Reproduced with permission from ref. 91 (Copyright 2022, The Royal Society of Chemistry) (f) DFT calculated highest occupied valence band (HOVB) and lowest unoccupied conduction band (LUCB) topologies of MOM. (g) Proposed visible-driven photocatalytic mechanism of Ag-AgMOM. (h) Hydrogen generation rate under 300 W irradiation in the presence of Ag-AgMOM synthesized at reaction time of 1 h, 20 h and 28 h with or without a 420 nm long-pass filter, respectively. Reproduced with permission from ref. 92 (Copyright 2023, Springer Nature).

increases the conductivity and light absorption of COFs. Therefore, tuning the π-electron structure and conjugation degree between the monomer and linker can effectively control the optoelectronic properties of COFs. For example, TP-EDDA and TP-BDDA COFs were synthesized using acetylene (–C≡C–) and dialkyne (–C≡C–C≡C–) linkers, respectively (Fig. 6a).[99] The edge absorption wavelengths of the two COFs were red-shifted by 20 and 25 nm, respectively (Fig. 6b). This study suggests that the dialkyne moiety is responsible for high charge transfer mobility, making it easy for the photoexcited excitons to migrate to the surface of the photocatalyst. The average rate of hydrogen production for TP-BDDA was 324 μmol h^{-1} g^{-1}, while no distinguishable hydrogen production was observed for TP-EDDA and TP-DTP COFs (Fig. 6c). When the degree of conjugation between the monomer and linker is weakened, it leads to lower crystallinity and poorer charge carrier behavior. For example, when the imine sonoCOF-F2 was converted to an acylamide-linked COF, the crystallinity decreased, and electron conjugation was lost,[100] resulting in decreased photocatalytic activity. However, after introducing benzyl alcohol to reduce the destruction of the imine bonds, the photo-stability of sonoCOF-F2 was enhanced.

Investigating exciton dynamics in COFs for photocatalytic hydrogen production presents challenges. These challenges arise from the poor optical quality of COF samples, caused by their insolubility and the difficulty in obtaining colloidal suspensions, which complicates optical characterization, particularly the acquisition of absorption spectra.[101] Nevertheless, a universal model of the electronic processes and optical properties of a series of imine-linked COFs was obtained through the study of electronic processes and optical properties of imine-linked COFs by highly sensitive optical spectroscopy techniques (PL, PDS and TA).[102] After photoexcitation, the initially generated singlet state undergoes singlet–singlet annihilation at a high rate, indicating that the initially produced excitons may be significantly delocalized, resulting in fast bimolecular processes. The singlet–singlet annihilation process generates trapped free charges, producing long-lived charges lasting from tens to hundreds of microseconds (Fig. 6d–f). This physical model is of reference value for designing COFs for photocatalytic HER.[90]

5.2.2 Polymer carbon nitride (PCN). Polymer carbon nitride (PCN) has garnered significant attention in the field of photocatalytic hydrogen production, with considerable advancements

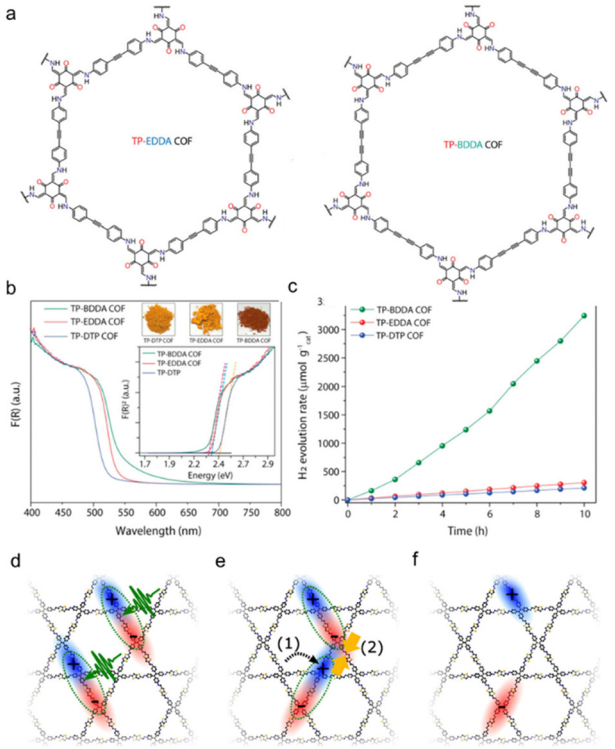

Fig. 6 (a) Scheme of the synthesis of TP-EDDA and TP-BDDA COFs (b) UV-vis diffuse reflectance spectra of TP-BDDA, TP-EDDA, and TP-DTP. The inset shows Tauc plots and optical images of the COF powders. (c) Photocatalytic hydrogen evolution performance of TP-BDDA, TP-EDDA, and TP-DTP catalysts under visible light irradiation ($\geq$395 nm) using TEOA as sacrificial agent. Reproduced with permission from ref. 99 (Copyright 2018, American Chemical Society). Model of the photoinduced electronic processes in COFs. (d) Absorption of photons leads to the formation of singlet excitons. (e) These singlets diffuse through the conjugated network (1) and can eventually collide with another one (2), *i.e.*, singlet–singlet annihilation. This process results in free charges (f) which eventually locate onto isolated, trap-like states leading to long lifetimes over tens of microseconds. Reproduced with permission from ref. 90 (Copyright 2022, American Chemical Society).

in structural design, synthesis, understanding of photocatalytic hydrogen production mechanisms, and performance research.[74] While many reviews have addressed the progress of PCN in photocatalysis,[103–106] this paper specifically emphasizes the crystallinity and tunability of PCN.

Crystallinity. Researchers have been committed to improving the crystallinity of PCN in order to enhance photocatalytic activity and characterization.[107–109] PCN synthesized by traditional thermal-induced polymerization typically exhibits low crystallinity, due to the high thermodynamic activity of nitrogen, which tends to form molecular nitrogen even at moderately elevated temperatures. LiCl–KCl eutectic mixture has good solvating properties for nitrides, carbides, cyanides, cyanates, and thiocyanates. Inspired by this, ionothermal methods have been used to synthesize PCN with higher crystallinity at high temperatures. In 2008, a lithium ion and chlorine ion-embedded molten salt method was reported to produce heptazine PCN that exhibited many well-resolved and strong X-ray diffraction patterns,[110] as shown in Fig. 7a. The space group and cell parameters were determined to be P 6 3 cm (185) based on XRD results. Scanning electron microscopy (SEM) images show the formation of hexagonal prisms, indicating the inherent single-crystal characteristics of CN. Clear lattice fringes were obtained from high-resolution transmission electron microscopy (HRTEM) images (Fig. 7b and c), and the interplanar spacing was consistent with XRD analysis. Two-dimensional triazine-based carbon nitride crystalline films were obtained by ionothermal interfacial reaction (Fig. 7d),[111] and ordered triazine crystallinity was observed by aberration-corrected transmission electron microscopy (Fig. 7e and f). Although these highly crystalline PCNs have not been used in photocatalytic reactions, they are useful for exploring photocatalytic mechanisms.

In 2020, a study was reported that revealed the photocatalytic active surface of PCN based on highly crystalline PTI/Li^+Cl^- structures. Due to their high degree of crystallinity (Fig. 8a and b), they are relatively stable under high-energy electron beam irradiation, enabling characterization of the photocatalytic process using high-angle annular dark-field scanning transmission electron microscopy, energy dispersive spectroscopy, and aberration-corrected imaging (Fig. 8c). In the photodeposition experiments, it was found that Pt tends to deposit on the edges of Pt clusters, specifically on the $\{10\bar{1}0\}$ plane as shown in Fig. 8d–f. PTI/Li^+Cl^- crystals with different aspect ratios were further prepared, and their overall water-splitting performance was found to be linearly related to the relative surface area of the $\{10\bar{1}0\}$ and {0001} planes. PTI-550, which has more $\{10\bar{1}0\}$ exposed crystal planes, achieved maximum hydrogen and oxygen evolution rates of 189 and 91 μmol h^{-1}, respectively (Fig. 8g). Therefore, this study indicates that the prism $\{10\bar{1}0\}$ plane is more active than the basal {0001} plane.[67] Highly crystalline PCNs provide conditions for investigating the photocatalytic active surfaces, but the study of the exciton generation and transfer processes in PCNs is still scarce and requires spectroscopic characterization.

Tunability. The local molecular structure of PCN plays a critical role in determining its physicochemical properties, which subsequently influence its performance and potential applications. Consequently, modulating the molecular structure of PCN serves as a crucial approach to enhance its performance. PCN not only possesses numerous polymer properties and characteristics akin to graphite-like materials but also exhibits unique in-plane voids and intralayer hydrogen bonds, offering a multitude of possibilities for tunability in carbon nitride materials.

Due to the bottom-up synthesis approach of PCN, its electronic structure, molecular, and structural architecture can be tailored not only by copolymerizing another structurally compatible organic group with the CN precursor but also by incorporating external impurities into the CN framework. Various atoms, including B,[113,114] C,[115,116] O,[117,118] F,[119] and P,[120] have been integrated into the CN structure. Among these,

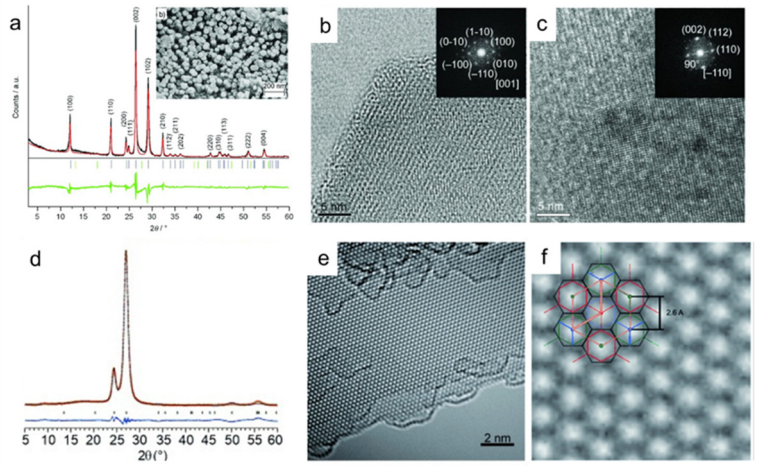

Fig. 7 Physical characterization of crystalline graphitic carbon nitride as obtained from the quartz glass ampoule (salt-melt reaction). (a) Le Bail decomposition and refinement performed on the XRD pattern of g-C_3N_4. (b) and (c) High-resolution TEM images showing a view in [001] direction and a view of the [−110] zone of g-C_3N_4, respectively. Reproduced with permission from ref. 110 (Copyright 2008, Wiley-VCH). (d) X-Ray analysis of TGCN with the observed pattern in red, the refined profile in black, the difference plot in blue, and Bragg peak positions in green. (e and f) Mechanically cleaved layers of TGCN as imaged by high-resolution TEM. Reproduced with permission from ref. 111 (Copyright 2014, Wiley-VCH).

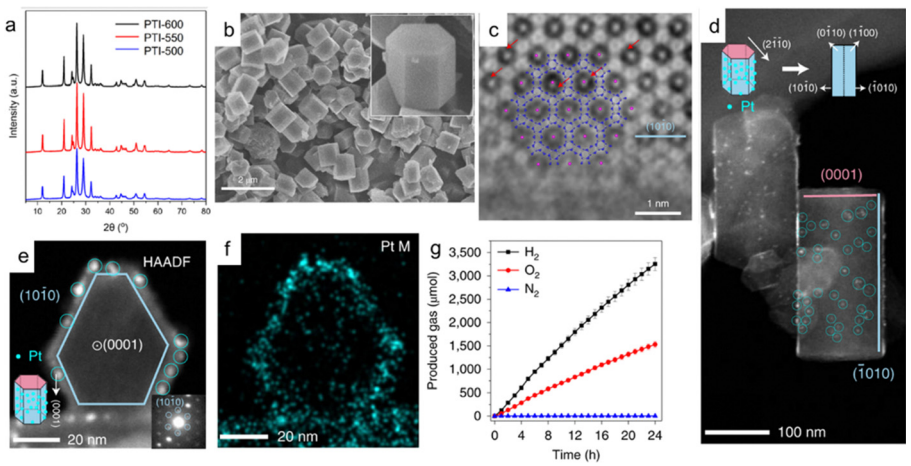

Fig. 8 (a) PXRD patterns of PTI samples. (b) SEM image showing the well-developed prism-like shape of PTI/Li^+Cl^- crystals. The inset shows the expanded view of a crystal. (c) The AC-iDPC images of a typical PTI/Li^+Cl^- crystal aligned along the [0001] direction. The positions of C, N and Cl atoms are superimposed. Some typical Li ions are denoted by red arrows. (d) The HAADF-STEM image of a PTI crystal aligned to the [$2\bar{1}\bar{1}0$] direction. The inset shows a schematic illustration of the distribution of Pt particles on the surfaces of PTI crystals. The blue circles indicate the positions of Pt particles. (e) The HAADF-STEM image of a PTI crystal aligned close to the [0001] direction; the inset shows the diffraction pattern from the particle. Note that the side faces correspond to the {$10\bar{1}0$} facets. (f) EDS maps of the main Pt elements. (g) The accumulated amount of the gases produced by PTI-550 (evacuated at each hour after sampling). The error bars show standard deviation. Reproduced with permission from ref. 111 (Copyright 2020, Springer Nature).

B-doped PCN is a notable example,[112] designed and synthesized as ultra-thin PCN and B-doped PCN (BDCNN) layers that electrostatically self-assemble into a 2D/2D Z-type heterostructure for photocatalytic water splitting (Fig. 9a). Considering the relatively large energy gap (~2.72 eV) of PCN, which limits visible light absorption, the narrow bandgap BDCNN is employed as a hydrogen evolution catalyst and combined with another BDCNN layer as an oxygen evolution component (Fig. 9b). This enhances the performance of photocatalytic water splitting, achieving a solar-to-hydrogen conversion efficiency of 1.16% under one-sun illumination (Fig. 9c).

Analogous to graphene, carbon nanotubes, and other carbon nanostructures, chemical modification of PCN serves as an efficient method to introduce various functional moieties onto the outer surface of PCN.[121] Due to the incomplete condensation or polymerization in pristine PCN, ample amino groups persist on the edge planes, enabling the direct incorporation of functional groups into the PCN framework. $NaBH_4$ can be thermally decomposed to generate hydrogen, introducing cyano end groups as electron acceptors into PCN structures.[122] The as-prepared PCN exhibits both p-type and n-type conductivity. This homojunction structure facilitates charge transfer

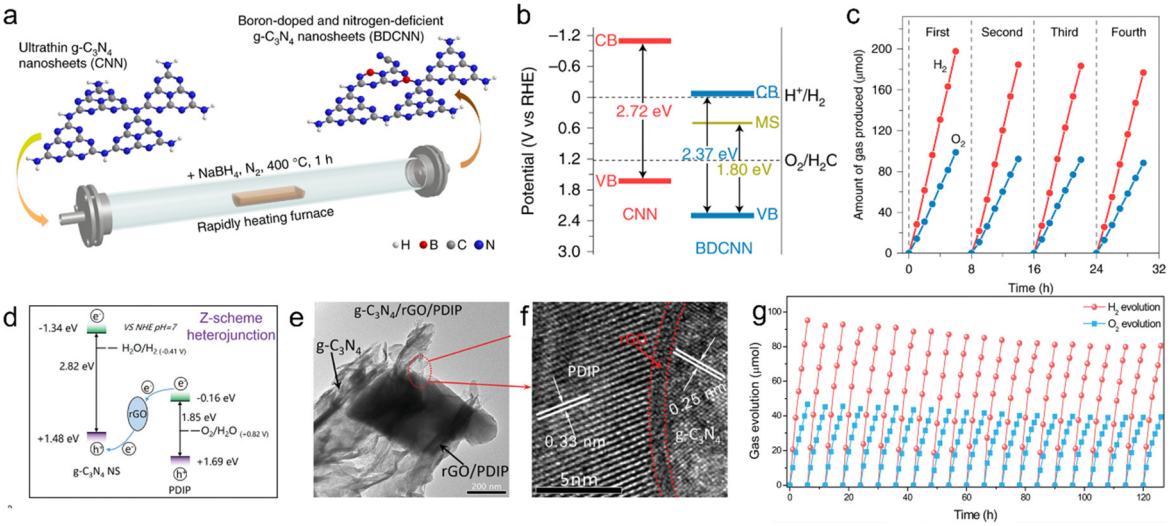

Fig. 9 Tunability of PCN. (a) Schematic of the synthesis of BDCNN derived from CNN. (b) Band structure alignments for CNN and BDCNN. (c) Cycling of photocatalytic overall water splitting over CNN/BDCNN, where each cycle was started with a one-hour argon flush. Reaction conditions: 40 mg photocatalyst, 0.9 wt% Pt and 3.0 wt% $Co(OH)_2$ co-catalysts were loaded onto CNN and BDCNN, respectively. Reproduced with permission from ref. 112 (Copyright 2021, Springer Nature). (d) The schematic Z-scheme charge transfer mechanism. (e) TEM image and (f) the corresponding HRTEM image of PCN/rGO/PDIP. (g) The repeated cycles of photocatalytic overall water splitting. Reproduced with permission from ref. 124 (Copyright 2021, Wiley-VCH).

and separation, resulting in an enhancement in photocatalytic HER.

However, covalent modification can damage the sp^2-dominated structure of PCN, leading to defects and the loss of electronic properties. In contrast, non-covalent functionalization is generally preferred, as it preserves the structure and electronic properties of PCN while simultaneously binding PCN to various substances, such as polymers, aromatic molecules, and graphene.[123] These non-covalent interactions encompass π–π stacking, electrostatic interactions, and hydrogen bonding. For instance, reduced graphene can also engage in efficient π–π stacking interactions with PCN. Our group successfully constructed a PCN/rGO/PDIP Z scheme to achieve efficient photocatalytic water splitting, as shown in Fig. 9d–f.[124] A substantial internal electric field is established, which enhances charge separation efficiency by 8.5 times. PCN/rGO/PDIP exhibited efficient photocatalytic OWS with H_2 and O_2 release rates of 15.80 and 7.80 μmol h^{-1}, respectively. Concurrently, AQY of 4.94% at 420 nm and STH of 0.30% were achieved, surpassing many reported PCN-based photocatalysts. And no notable deactivation emerged during continuous measurement for more than 120 h (Fig. 9g).

6. Efficiency and stability of organic semiconductors for photocatalytic HER

6.1 Evaluation standard

It is common practice to report HER values in mmol g^{-1} h^{-1} units, which facilitates more effective comparisons among different photocatalysts than using mmol h^{-1}. When comparing the HER activity of various photocatalysts, it is essential to consider the mass distribution of the photocatalyst dispersed in the liquid. For suspended photocatalysts, an optimal mass of photocatalyst per liquid volume is required to achieve the highest HER. Excessive amounts lead to light scattering, while insufficient amounts result in unsaturated light utilization. Consequently, it is necessary to test hydrogen production rates at different photocatalyst loadings to identify the optimal amount.[2,4,5] The HER rates are comparable among different photocatalysts at the optimum photocatalyst dosing. It is important to note that the determining factor for optimal loading is the extinction coefficient of the photocatalyst. Organic photocatalysts typically exhibit a high extinction coefficient, attributed to the extensive π-conjugation and strong intramolecular charge transfer of organic semiconductor materials.[125,126] This provides a foundation for efficient photon utilization, implying that light absorption saturation can be achieved at lower loadings. Furthermore, as the measured gas release rate varies with experimental conditions and the light source employed, it is necessary to report AQE and/or STH values for specific wavelengths.[127] However, when hydrogen production occurs at the expense of the donor, the efficiency of organic photocatalysts is comparable to that of inorganic ones.

6.2 Efficiency

The reported STH efficiency of the state-of-the-art PCN system is 1.16%,[112] while the highest documented STH efficiency for covalent organic frameworks (COFs) is 0.40%,[128] despite their generally broader light absorption range. In the case of metal–organic frameworks (MOFs), organic ligands in these materials are susceptible to replacement by water molecules in aqueous environments, potentially causing framework collapse. To date, no reports on the STH efficiency of MOFs have been published, possibly due to challenges in quantifying their low activity.

It is evident that the STH efficiencies of widely studied PCN, MOF, and COF organic photocatalysts are considerably lower than the target STH of 10%. This underscores the difficulty in constructing a complete water-splitting system using only organic photocatalysts. However, organic photocatalysts remain promising due to their tunable band structures, providing opportunities for further research and development to enhance their efficiency and stability in photocatalytic water-splitting applications. Persistent investigation and optimization of these materials may eventually yield photocatalysts that approach or surpass the desired STH efficiency, advancing the field toward greener and more sustainable energy solutions.

6.3 Photocatalyst stability

For conjugated supramolecular organic photocatalysts, aggregate formation relies on π–π interactions, hydrogen bonding, and other non-covalent interactions. In a dispersion environment, factors such as temperature, pH, and co-existing ions may all influence the stability of hydrogen bonding. Consequently, the sensitivity of catalyst morphology and crystalline phase to the dispersion environment increases when the formation of supramolecular aggregates is not primarily driven by π–π interactions.[129,130]

This may be due to supramolecular photocatalysts being relatively new in HER applications, resulting in limited attention given to studying their stability in dispersions. For the few, we have discussed the stability in the aqueous phase when reporting on PTA supramolecular nanosheet photocatalysts.[45] For MOF photocatalysts, the aqueous stability in photocatalytic HERs requires further review, as metal–ligand coordination interactions are strongly influenced by water.[131] In contrast, polymer photocatalysts linked by covalent bonds exhibit better chemical stability. Several studies have reported that the XRD patterns of conjugated organic frameworks (COFs) linked by olefins remained relatively unchanged after immersion in strong acidic and alkaline environments.[132,133] Moreover, the stability of photocatalysts may be affected by cavity oxidation in the absence of a sacrificial agent in the dispersion, leading to corrosion, leakage, and reduced photostability of the catalyst. Therefore, when evaluating photocatalyst performance, it is crucial to consider their stability and sustainability in real-world application environments.

Organic photocatalysts typically contain conjugated structures in which π electrons can absorb photons, be excited to high energy levels, and form excited states. However, the energy of these excited states is usually high, leading to reactions with surrounding molecules that produce highly reactive species such as radicals and ions, which can easily cause oxidation and degradation of organic semiconductor materials. This can manifest as morphological changes and crystal phase transitions, a form of corrosion.[134,135] In contrast, inorganic semiconductors generally consist of a single element or a few elements, and their structures are relatively simple, resulting in lower corrosivity. Additionally, impurities and defects between organic molecules can also produce highly reactive species under light, leading to photodegradation of organic semiconductors. Increasing the crystallinity of organic semiconductors can reduce the presence of internal defects and impurities, thereby improving the stability of the material. More importantly, high crystallinity reduces the accumulation of charge carriers in localized regions of organic semiconductors, consequently decreasing their reactivity towards the crystal itself. Furthermore, avoiding the use of overly strong light sources or prolonged exposure to light can also reduce the occurrence of photodegradation.

7. Conclusion

Despite significant advancements in the development of novel organic semiconductors for photocatalytic HER, there remain four major challenges to overcome in this field.

The first challenge pertains to the photophysical characterization of organic semiconductors. Due to their low tolerance for high-energy electrons and molecular packing properties, characterizing organic semiconductors using electron microscopy and *in situ* methods proves difficult.

The second challenge involves distinguishing exciton and charge carrier behavior in organic semiconductors. Given the complexity of the electronic structure and limitations in characterization methods, the migration and diffusion of excitons, as well as the separation process, remain contentious issues.

The third challenge concerns the long-term stability of organic semiconductors under operating conditions. Although polymer stability has been demonstrated for at least a few consecutive days in the absence of sacrificial donors, most organic semiconductors are susceptible to photodegradation. Hence, strategies beyond improving crystallinity should be explored.

The fourth challenge is to develop photocatalytic HER systems that do not rely on hole scavengers. Thus far, there are relatively few organic photocatalyst systems for efficient OWS. The full potential of cost-effective, tunable, and flexible organic photocatalysts can only be realized when the STH efficiency matches that of inorganic photocatalysts.

Conflicts of interest

The authors declare no competing interests.

Acknowledgements

This work was supported by National Natural Science Foundation of China (21872077), National Key Research and Development Program of China (2020YFA0710304), and Collaborative Innovation Center for Regional Environmental Quality.

References

1 P. Zhou, I. A. Navid, Y. Ma, Y. Xiao, P. Wang, Z. Ye, B. Zhou, K. Sun and Z. Mi, Solar-to-hydrogen efficiency of more than

9% in photocatalytic water splitting, *Nature*, 2023, **613**(7942), 66–70.

2 L. Liu, H. Meng, Y. Chai, X. Chen, J. Xu, X. Liu, W. Liu, D. M. Guldi and Y. Zhu, Enhancing Built-in Electric Fields for Efficient Photocatalytic Hydrogen Evolution by Encapsulating C60 Fullerene into Zirconium-Based Metal–Organic Frameworks, *Angew. Chem., Int. Ed.*, 2023, e202217897.

3 S. L. Lee and C. J. Chang, Recent Developments about Conductive Polymer Based Composite Photocatalysts, *Polymers*, 2019, **11**(2), 21.

4 J. Xu, W. Li, W. Liu, J. Jing, K. Zhang, L. Liu, J. Yang, E. Zhu, J. Li and Y. Zhu, Efficient Photocatalytic Hydrogen and Oxygen Evolution by Side-Group Engineered Benzodiimidazole Oligomers with Strong Built-in Electric Fields and Short-Range Crystallinity, *Angew. Chem., Int. Ed.*, 2022, **61**(45), e202212243.

5 J. Yang, J. Jing, W. Li and Y. Zhu, Electron Donor–Acceptor Interface of TPPS/PDI Boosting Charge Transfer for Efficient Photocatalytic Hydrogen Evolution, *Adv. Sci.*, 2022, **9**(17), 2201134.

6 X. Xu, Y. Zhao and Y. Liu, Wearable Electronics Based on Stretchable Organic Semiconductors, *Small*, 2023, 2206309.

7 D. Wang, L. Lu, Z. Zhao, K. Zhao, X. Zhao, C. Pu, Y. Li, P. Xu, X. Chen, Y. Guo, L. Suo, J. Liang, Y. Cui and Y. Liu, Large area polymer semiconductor sub-microwire arrays by coaxial focused electrohydrodynamic jet printing for high-performance OFETs, *Nat. Commun.*, 2022, **13**(1), 6214.

8 K. Chen, J. Xiao, J. J. M. Vequizo, T. Hisatomi, Y. Ma, M. Nakabayashi, T. Takata, A. Yamakata, N. Shibata and K. Domen, Overall Water Splitting by a SrTaO2N-Based Photocatalyst Decorated with an Ir-Promoted Ru-Based Cocatalyst, *J. Am. Chem. Soc.*, 2023, **145**(7), 3839–3843.

9 D. Zhang, J. Teng, H. Yang, Z. Fang, K. Song, L. Wang, H. Hou, X. Lu, C. R. Bowen and W. Yang, Air-condition process for scalable fabrication of CdS/ZnS 1D/2D heterojunctions toward efficient and stable photocatalytic hydrogen production, *Carbon Energy*, 2022, 1–14.

10 M. Liu, Y. Chen, J. Su, J. Shi, X. Wang and L. Guo, Photocatalytic hydrogen production using twinned nanocrystals and an unanchored NiSx co-catalyst, *Nat. Energy*, 2016, **1**(11), 16151.

11 H. Nishiyama, T. Yamada, M. Nakabayashi, Y. Maehara, M. Yamaguchi, Y. Kuromiya, Y. Nagatsuma, H. Tokudome, S. Akiyama, T. Watanabe, R. Narushima, S. Okunaka, N. Shibata, T. Takata, T. Hisatomi and K. Domen, Photocatalytic solar hydrogen production from water on a 100-m2 scale, *Nature*, 2021, **598**(7880), 304–307.

12 T. Takata, J. Jiang, Y. Sakata, M. Nakabayashi, N. Shibata, V. Nandal, K. Seki, T. Hisatomi and K. Domen, Photocatalytic water splitting with a quantum efficiency of almost unity, *Nature*, 2020, **581**(7809), 411–414.

13 T. He, M. Stolte, Y. Wang, R. Renner, P. P. Ruden, F. Würthner and C. D. Frisbie, Site-specific chemical doping reveals electron atmospheres at the surfaces of organic semiconductor crystals, *Nat. Mater.*, 2021, **20**(11), 1532–1538.

14 N. Serpone, A. V. Emeline, V. K. Ryabchuk, V. N. Kuznetsov, Y. M. Artem'ev and S. Horikoshi, Why do Hydrogen and Oxygen Yields from Semiconductor-Based Photocatalyzed Water Splitting Remain Disappointingly Low? Intrinsic and Extrinsic Factors Impacting Surface Redox Reactions, *ACS Energy Lett.*, 2016, **1**(5), 931–948.

15 P. V. Kamat and S. Jin, Semiconductor Photocatalysis: ''Tell Us the Complete Story!'', *ACS Energy Lett.*, 2018, **3**(3), 622–623.

16 J. Schneider and D. W. Bahnemann, Undesired Role of Sacrificial Reagents in Photocatalysis, *J. Phys. Chem. Lett.*, 2013, **4**(20), 3479–3483.

17 Y. Yang, X. Chu, H.-Y. Zhang, R. Zhang, Y.-H. Liu, F.-M. Zhang, M. Lu, Z.-D. Yang and Y.-Q. Lan, Engineering β-ketoamine covalent organic frameworks for photocatalytic overall water splitting, *Nat. Commun.*, 2023, **14**(1), 593.

18 J. Zhang, T. Bai, H. Huang, M.-H. Yu, X. Fan, Z. Chang and X.-H. Bu, Metal–Organic-Framework-Based Photocatalysts Optimized by Spatially Separated Cocatalysts for Overall Water Splitting, *Adv. Mater.*, 2020, **32**(49), 2004747.

19 H. Zhao, Q. Mao, L. Jian, Y. Dong and Y. Zhu, Photodeposition of earth-abundant cocatalysts in photocatalytic water splitting: Methods, functions, and mechanisms, *Chin. J. Catal.*, 2022, **43**(7), 1774–1804.

20 H. Zhao, L. Jian, M. Gong, M. Jing, H. Li, Q. Mao, T. Lu, Y. Guo, R. Ji, W. Chi, Y. Dong and Y. Zhu, Transition-Metal-Based Cocatalysts for Photocatalytic Water Splitting, *Small Struct.*, 2022, **3**(7), 2100229.

21 Y. Li, Z. Wang, T. Xia, H. Ju, K. Zhang, R. Long, Q. Xu, C. Wang, L. Song, J. Zhu, J. Jiang and Y. Xiong, Implementing Metal-to-Ligand Charge Transfer in Organic Semiconductor for Improved Visible-Near-Infrared Photocatalysis, *Adv. Mater.*, 2016, **28**(32), 6959–6965.

22 X. Li, W. Bi, L. Zhang, S. Tao, W. Chu, Q. Zhang, Y. Luo, C. Wu and Y. Xie, Single-Atom Pt as Co-Catalyst for Enhanced Photocatalytic H2 Evolution, *Adv. Mater.*, 2016, **28**(12), 2427–2431.

23 L. Wang, R. Tang, A. Kheradmand, Y. Jiang, H. Wang, W. Yang, Z. Chen, X. Zhong, S. P. Ringer, X. Liao, W. Liang and J. Huang, Enhanced solar-driven benzaldehyde oxidation with simultaneous hydrogen production on Pt single-atom catalyst, *Appl. Catal., B*, 2021, **284**, 119759.

24 P. Zhou, N. Li, Y. Chao, W. Zhang, F. Lv, K. Wang, W. Yang, P. Gao and S. Guo, Thermolysis of Noble Metal Nanoparticles into Electron-Rich Phosphorus-Coordinated Noble Metal Single Atoms at Low Temperature, *Angew. Chem., Int. Ed.*, 2019, **58**(40), 14184–14188.

25 S. Cao, H. Li, T. Tong, H.-C. Chen, A. Yu, J. Yu and H. M. Chen, Single-Atom Engineering of Directional Charge Transfer Channels and Active Sites for Photocatalytic Hydrogen Evolution, *Adv. Funct. Mater.*, 2018, **28**(32), 1802169.

26 Z. Chen, Y. Bu, L. Wang, X. Wang and J.-P. Ao, Single-sites Rh-phosphide modified carbon nitride photocatalyst for boosting hydrogen evolution under visible light, *Appl. Catal., B*, 2020, **274**, 119117.

27 L. Zeng, C. Dai, B. Liu and C. Xue, Oxygen-assisted stabilization of single-atom Au during photocatalytic hydrogen evolution, *J. Mater. Chem. A*, 2019, **7**(42), 24217–24221.
28 X. Li, S. Zhao, X. Duan, H. Zhang, S.-Z. Yang, P. Zhang, S. P. Jiang, S. Liu, H. Sun and S. Wang, Coupling hydrothermal and photothermal single-atom catalysis toward excellent water splitting to hydrogen, *Appl. Catal., B*, 2021, **283**, 119660.
29 W. Zhang, Q. Peng, L. Shi, Q. Yao, X. Wang, A. Yu, Z. Chen and Y. Fu, Merging Single-Atom-Dispersed Iron and Graphitic Carbon Nitride to a Joint Electronic System for High-Efficiency Photocatalytic Hydrogen Evolution, *Small*, 2019, **15**(50), 1905166.
30 Y. Cao, S. Chen, Q. Luo, H. Yan, Y. Lin, W. Liu, L. Cao, J. Lu, J. Yang, T. Yao and S. Wei, Atomic-Level Insight into Optimizing the Hydrogen Evolution Pathway over a Co1-N4 Single-Site Photocatalyst, *Angew. Chem., Int. Ed.*, 2017, **56**(40), 12191–12196.
31 Y. Li, Y. Wang, C.-L. Dong, Y.-C. Huang, J. Chen, Z. Zhang, F. Meng, Q. Zhang, Y. Huangfu, D. Zhao, L. Gu and S. Shen, Single-atom nickel terminating sp2 and sp3 nitride in polymeric carbon nitride for visible-light photocatalytic overall water splitting, *Chem. Sci.*, 2021, **12**(10), 3633–3643.
32 R. Qi, P. Yu, J. Zhang, W. Guo, Y. He, H. Hojo, H. Einaga, Q. Zhang, X. Liu, Z. Jiang and W. Shangguan, Efficient visible light photocatalysis enabled by the interaction between dual cooperative defect sites, *Appl. Catal., B*, 2020, **274**, 119099.
33 W. Jiang, Y. Zhao, X. Zong, H. Nie, L. Niu, L. An, D. Qu, X. Wang, Z. Kang and Z. Sun, Photocatalyst for High-Performance H2 Production: Ga-Doped Polymeric Carbon Nitride, *Angew. Chem., Int. Ed.*, 2021, **60**(11), 6124–6129.
34 Z. Xu, M. G. Kibria, B. AlOtaibi, P. N. Duchesne, L. V. Besteiro, Y. Gao, Q. Zhang, Z. Mi, P. Zhang, A. O. Govorov, L. Mai, M. Chaker and D. Ma, Towards enhancing photocatalytic hydrogen generation: Which is more important, alloy synergistic effect or plasmonic effect?, *Appl. Catal., B*, 2018, **221**, 77–85.
35 K. Bhunia, M. Chandra, S. Khilari and D. Pradhan, Bimetallic PtAu Alloy Nanoparticles-Integrated g-C3N4 Hybrid as an Efficient Photocatalyst for Water-to-Hydrogen Conversion, *ACS Appl. Mater. Interfaces*, 2019, **11**(1), 478–488.
36 C. Han, L. Wu, L. Ge, Y. Li and Z. Zhao, AuPd bimetallic nanoparticles decorated graphitic carbon nitride for highly efficient reduction of water to H2 under visible light irradiation, *Carbon N Y*, 2015, **92**, 31–40.
37 S. Bai, L. Yang, C. Wang, Y. Lin, J. Lu, J. Jiang and Y. Xiong, Boosting Photocatalytic Water Splitting: Interfacial Charge Polarization in Atomically Controlled Core–Shell Cocatalysts, *Angew. Chem., Int. Ed.*, 2015, **54**(49), 14810–14814.
38 S. Chen, M. Li, S. Yang, X. Li and S. Zhang, Graphitied carbon-coated bimetallic FeCu nanoparticles as original g-C3N4 cocatalysts for improving photocatalystic activity, *Appl. Surf. Sci.*, 2019, **492**, 571–578.
39 Z. Jin and L. Zhang, Performance of Ni-Cu bimetallic co-catalyst g-C3N4 nanosheets for improving hydrogen evolution, *J. Mater. Sci. Technol.*, 2020, **49**, 144–156.
40 X. Han, D. Xu, L. An, C. Hou, Y. Li, Q. Zhang and H. Wang, Ni-Mo nanoparticles as co-catalyst for drastically enhanced photocatalytic hydrogen production activity over g-C3N4, *Appl. Catal., B*, 2019, **243**, 136–144.
41 G. Zhang, Q. Ji, Z. Wu, G. Wang, H. Liu, J. Qu and J. Li, Facile ''Spot-Heating'' Synthesis of Carbon Dots/Carbon Nitride for Solar Hydrogen Evolution Synchronously with Contaminant Decomposition, *Adv. Funct. Mater.*, 2018, **28**(14), 1706462.
42 M. Zhu, S. Kim, L. Mao, M. Fujitsuka, J. Zhang, X. Wang and T. Majima, Metal-Free Photocatalyst for H_2 Evolution in Visible to Near-Infrared Region: Black Phosphorus/Graphitic Carbon Nitride, *J. Am. Chem. Soc.*, 2017, **139**(37), 13234–13242.
43 R. S. Sprick, J.-X. Jiang, B. Bonillo, S. Ren, T. Ratvijitvech, P. Guiglion, M. A. Zwijnenburg, D. J. Adams and A. I. Cooper, Tunable Organic Photocatalysts for Visible-Light-Driven Hydrogen Evolution, *J. Am. Chem. Soc.*, 2015, **137**(9), 3265–3270.
44 S. Bi, C. Yang, W. Zhang, J. Xu, L. Liu, D. Wu, X. Wang, Y. Han, Q. Liang and F. Zhang, Two-dimensional semiconducting covalent organic frameworks via condensation at arylmethyl carbon atoms, *Nat. Commun.*, 2019, **10**(1), 2467.
45 Y. Guo, Q. Zhou, J. Nan, W. Shi, F. Cui and Y. Zhu, Perylenetetracarboxylic acid nanosheets with internal electric fields and anisotropic charge migration for photocatalytic hydrogen evolution, *Nat. Commun.*, 2022, **13**(1), 2067.
46 S. Fratini, M. Nikolka, A. Salleo, G. Schweicher and H. Sirringhaus, Charge transport in high-mobility conjugated polymers and molecular semiconductors, *Nat. Mater.*, 2020, **19**(5), 491–502.
47 C. Wang, H. Dong, L. Jiang and W. Hu, Organic semiconductor crystals, *Chem. Soc. Rev.*, 2018, **47**(2), 422–500.
48 E. Jin, K. Geng, S. Fu, S. Yang, N. Kanlayakan, M. A. Addicoat, N. Kungwan, J. Geurs, H. Xu, M. Bonn, H. I. Wang, J. Smet, T. Kowalczyk and D. Jiang, Exceptional electron conduction in two-dimensional covalent organic frameworks, *Chem*, 2021, **7**(12), 3309–3324.
49 H. Sato, S. A. A. Rahman, Y. Yamada, H. Ishii and H. Yoshida, Conduction band structure of high-mobility organic semiconductors and partially dressed polaron formation, *Nat. Mater.*, 2022, **21**(8), 910–916.
50 R. Dong, P. Han, H. Arora, M. Ballabio, M. Karakus, Z. Zhang, C. Shekhar, P. Adler, P. S. Petkov, A. Erbe, S. C. B. Mannsfeld, C. Felser, T. Heine, M. Bonn, X. Feng and E. Cánovas, High-mobility band-like charge transport in a semiconducting two-dimensional metal–organic framework, *Nat. Mater.*, 2018, **17**(11), 1027–1032.
51 M. B. Price, P. A. Hume, A. Ilina, I. Wagner, R. R. Tamming, K. E. Thorn, W. Jiao, A. Goldingay, P. J. Conaghan, G. Lakhwani, N. J. L. K. Davis, Y. Wang, P. Xue, H. Lu, K. Chen, X. Zhan and J. M. Hodgkiss, Free charge photogeneration in a single component high photovoltaic efficiency organic semiconductor, *Nat. Commun.*, 2022, **13**(1), 2827.

52 V. Settels, A. Schubert, M. Tafipolski, W. Liu, V. Stehr, A. K. Topczak, J. Pflaum, C. Deibel, R. F. Fink, V. Engel and B. Engels, Identification of Ultrafast Relaxation Processes As a Major Reason for Inefficient Exciton Diffusion in Perylene-Based Organic Semiconductors, *J. Am. Chem. Soc.*, 2014, **136**(26), 9327–9337.

53 H. Najafov, B. Lee, Q. Zhou, L. C. Feldman and V. Podzorov, Observation of long-range exciton diffusion in highly ordered organic semiconductors, *Nat. Mater.*, 2010, **9**(11), 938–943.

54 Y. Shan, J. Wang, Z. Guo, D. Liu, Y. Zhao, N. Lu and L. Li, Surface-Doping-Induced Mobility Modulation Effect for Transport Enhancement in Organic Single-Crystal Transistors, *Adv. Mater.*, 2023, **35**(3), 2205517.

55 O. V. Mikhnenko, P. W. M. Blom and T.-Q. Nguyen, Exciton diffusion in organic semiconductors, *Energy Environ. Sci.*, 2015, **8**(7), 1867–1888.

56 Y. Huang, D. L. Elder, A. L. Kwiram, S. A. Jenekhe, A. K. Y. Jen, L. R. Dalton and C. K. Luscombe, Organic Semiconductors at the University of Washington: Advancements in Materials Design and Synthesis and toward Industrial Scale Production, *Adv. Mater.*, 2021, **33**(22), 1904239.

57 Y. Guo, W. Shi and Y. Zhu, Electric field engineering for steering photogenerated charge separation and enhancing photoactivity, *EcoMat*, 2019, **2**, 12007.

58 M. T. Dang, L. Hirsch, G. Wantz and J. D. Wuest, Controlling the Morphology and Performance of Bulk Heterojunctions in Solar Cells. Lessons Learned from the Benchmark Poly(3-hexylthiophene):[6,6]-Phenyl-C61-butyric Acid Methyl Ester System, *Chem. Rev.*, 2013, **113**(5), 3734–3765.

59 A. J. Heeger, 25th Anniversary Article: Bulk Heterojunction Solar Cells: Understanding the Mechanism of Operation, *Adv. Mater.*, 2014, **26**(1), 10–28.

60 J. Nelson, Polymer:fullerene bulk heterojunction solar cells, *Mater. Today*, 2011, **14**(10), 462–470.

61 Y. Zhang, Y. Dai, H. Li, L. Yin and M. R. Hoffmann, Proton-assisted electron transfer and hydrogen-atom diffusion in a model system for photocatalytic hydrogen production, *Communi. Mater.*, 2020, **1**(1), 66.

62 L. Xu, B. Tian, T. Wang, Y. Yu, Y. Wu, J. Cui, Z. Cao, J. Wu, W. Zhang, Q. Zhang, J. Liu, Z. Li and Y. Tian, Direct Z-scheme polymeric heterojunction boosts photocatalytic hydrogen production via a rebuilt extended π-delocalized network, *Energy Environ. Sci.*, 2022, **15**(12), 5059–5068.

63 F. Sun, S. Tan, H.-J. Cao, C.-S. Lu, D. Tu, J. Poater, M. Solà and H. Yan, Facile Construction of New Hybrid Conjugation via Boron Cage Extension, *J. Am. Chem. Soc.*, 2023, **145**(6), 3577–3587.

64 L. Wang, W. Jiang, S. Guo, S. Wang, M. Zhang, Z. Liu, G. Wang, Y. Miao, L. Yan, J.-Y. Shao, Y.-W. Zhong, Z. Liu, D. Zhang, H. Fu and J. Yao, Robust singlet fission process in strong absorption π-expanded diketopyrrolopyrroles, *Chem. Sci.*, 2022, **13**(46), 13907–13913.

65 J. Jing, J. Yang, Z. Zhang and Y. Zhu, Supramolecular Zinc Porphyrin Photocatalyst with Strong Reduction Ability and Robust Built-In Electric Field for Highly Efficient Hydrogen Production, *Adv. Energy Mater.*, 2021, **11**(29), 2101392.

66 M. Schwarze, W. Tress, B. Beyer, F. Gao, R. Scholz, C. Poelking, K. Ortstein, A. A. Günther, D. Kasemann, D. Andrienko and K. Leo, Band structure engineering in organic semiconductors, *Science*, 2016, **352**(6292), 1446–1449.

67 L. Lin, Z. Lin, J. Zhang, X. Cai, W. Lin, Z. Yu and X. Wang, Molecular-level insights on the reactive facet of carbon nitride single crystals photocatalysing overall water splitting, *Nat. Catal.*, 2020, **3**(8), 649–655.

68 R. Chen, S. Pang, H. An, J. Zhu, S. Ye, Y. Gao, F. Fan and C. Li, Charge separation via asymmetric illumination in photocatalytic Cu_2O particles, *Nat. Energy*, 2018, **3**(8), 655–663.

69 Z. Luo, X. Ye, S. Zhang, S. Xue, C. Yang, Y. Hou, W. Xing, R. Yu, J. Sun, Z. Yu and X. Wang, Unveiling the charge transfer dynamics steered by built-in electric fields in BiOBr photocatalysts, *Nat. Commun.*, 2022, **13**(1), 2230.

70 F. Li, G.-F. Han, H.-J. Noh, J.-P. Jeon, I. Ahmad, S. Chen, C. Yang, Y. Bu, Z. Fu, Y. Lu and J.-B. Baek, Balancing hydrogen adsorption/desorption by orbital modulation for efficient hydrogen evolution catalysis, *Nat. Commun.*, 2019, **10**(1), 4060.

71 G.-L. Zhang, T.-Y. Yang, J. Zhang and Y.-H. Zhang, Clarifying the Active Site Role of meso-Carboxyphenyl Group for Free Base Porphyrins in Photocatalytic H2 Evolution Reaction, *ChemCatChem*, 2023, **15**(2), e202201271.

72 Y. Yuan, L. Zhou, H. Robatjazi, J. L. Bao, J. Zhou, A. Bayles, L. Yuan, M. Lou, M. Lou, S. Khatiwada, E. A. Carter, P. Nordlander and N. J. Halas, Earth-abundant photocatalyst for H2 generation from NH3 with light-emitting diode illumination, *Science*, 2022, **378**(6622), 889–893.

73 J.-X. Jian, Q. Liu, Z.-J. Li, F. Wang, X.-B. Li, C.-B. Li, B. Liu, Q.-Y. Meng, B. Chen, K. Feng, C.-H. Tung and L.-Z. Wu, Chitosan confinement enhances hydrogen photogeneration from a mimic of the diiron subsite of [FeFe]-hydrogenase, *Nat. Commun.*, 2013, **4**(1), 2695.

74 Q. Zhou, Y. Guo, Z. Ye, Y. Fu, Y. Guo and Y. Zhu, Carbon nitride photocatalyst with internal electric field induced photogenerated carriers spatial enrichment for enhanced photocatalytic water splitting, *Mater. Today*, 2022, **58**, 100–109.

75 P. Zhou, H. Chen, Y. Chao, Q. Zhang, W. Zhang, F. Lv, L. Gu, Q. Zhao, N. Wang, J. Wang and S. Guo, Single-atom Pt-I3 sites on all-inorganic Cs2SnI6 perovskite for efficient photocatalytic hydrogen production, *Nat. Commun.*, 2021, **12**(1), 4412.

76 X. He, G. Zhu, J. Yang, H. Chang, Q. Meng, H. Zhao, X. Zhou, S. Yue, Z. Wang, J. Shi, L. Gu, D. Yan and Y. Weng, Photogenerated Intrinsic Free Carriers in Small-molecule Organic Semiconductors Visualized by Ultrafast Spectroscopy, *Sci. Rep.*, 2015, **5**(1), 17076.

77 J. Guo, Y. Zeng, Y. Zhen, H. Geng, Z. Wang, Y. Yi, H. Dong and W. Hu, Non-Equal Ratio Cocrystal Engineering to Improve Charge Transport Characteristics of Organic Semiconductors: A Case Study on Indolo[2,3-a]carbazole, *Angew. Chem., Int. Ed.*, 2022, **61**(28), e202202336.

78 S. Fu, E. Jin, H. Hanayama, W. Zheng, H. Zhang, L. Di Virgilio, M. A. Addicoat, M. Mezger, A. Narita, M. Bonn, K. Müllen and H. I. Wang, Outstanding Charge Mobility by Band Transport in Two-Dimensional Semiconducting Covalent Organic Frameworks, *J. Am. Chem. Soc.*, 2022, **144**(16), 7489–7496.

79 C. Wang, H. Dong, W. Hu, Y. Liu and D. Zhu, Semiconducting π-Conjugated Systems in Field-Effect Transistors: A Material Odyssey of Organic Electronics, *Chem. Rev.*, 2012, **112**(4), 2208–2267.

80 M. Mas-Torrent and C. Rovira, Role of Molecular Order and Solid-State Structure in Organic Field-Effect Transistors, *Chem. Rev.*, 2011, **111**(8), 4833–4856.

81 F. J. M. Hoeben, P. Jonkheijm, E. W. Meijer and A. P. H. J. Schenning, About Supramolecular Assemblies of π-Conjugated Systems, *Chem. Rev.*, 2005, **105**(4), 1491–1546.

82 J.-H. Deng, J. Luo, Y.-L. Mao, S. Lai, Y.-N. Gong, D.-C. Zhong and T.-B. Lu, π–π stacking interactions: Non-negligible forces for stabilizing porous supramolecular frameworks, *Sci. Adv.*, 2020, **6**(2), eaax9976.

83 Z. Wang, C. J. Medforth and J. A. Shelnutt, Self-Metallization of Photocatalytic Porphyrin Nanotubes, *J. Am. Chem. Soc.*, 2004, **126**(51), 16720–16721.

84 P. Guo, P. Chen and M. Liu, One-Dimensional Porphyrin Nanoassemblies Assisted via Graphene Oxide: Sheetlike Functional Surfactant and Enhanced Photocatalytic Behaviors, *ACS Appl. Mater. Interfaces*, 2013, **5**(11), 5336–5345.

85 Z. Zhang, Y. Zhu, X. Chen, H. Zhang and J. Wang, A Full-Spectrum Metal-Free Porphyrin Supramolecular Photocatalyst for Dual Functions of Highly Efficient Hydrogen and Oxygen Evolution, *Adv. Mater.*, 2019, **31**(7), e1806626.

86 S. Kumar, J. Shukla, Y. Kumar and P. Mukhopadhyay, Electron-poor arylenediimides, *Org. Chem. Front.*, 2018, **5**(14), 2254–2276.

87 G. Gao, M. Chen, J. Roberts, M. Feng, C. Xiao, G. Zhang, S. Parkin, C. Risko and L. Zhang, Rational Functionalization of a C70 Buckybowl To Enable a C70:Buckybowl Cocrystal for Organic Semiconductor Applications, *J. Am. Chem. Soc.*, 2020, **142**(5), 2460–2470.

88 T. Lu and Q. Chen, A simple method of identifying π orbitals for non-planar systems and a protocol of studying π electronic structure, *Theor. Chem. Acc.*, 2020, **139**(2), 25.

89 N. Kolobov, M. G. Goesten and J. Gascon, Metal–Organic Frameworks: Molecules or Semiconductors in Photocatalysis?, *Angew. Chem., Int. Ed.*, 2021, **60**, 26038.

90 N. C. Flanders, M. S. Kirschner, P. Kim, T. J. Fauvell, A. M. Evans, W. Helweh, A. P. Spencer, R. D. Schaller, W. R. Dichtel and L. X. Chen, Large Exciton Diffusion Coefficients in Two-Dimensional Covalent Organic Frameworks with Different Domain Sizes Revealed by Ultrafast Exciton Dynamics, *J. Am. Chem. Soc.*, 2020, **142**(35), 14957–14965.

91 Y. Pan, J. Wang, S. Chen, W. Yang, C. Ding, A. Waseem and H.-L. Jiang, Linker engineering in metal–organic frameworks for dark photocatalysis, *Chem. Sci.*, 2022, **13**(22), 6696–6703.

92 Y. Liu, C.-H. Liu, T. Debnath, Y. Wang, D. Pohl, L. V. Besteiro, D. M. Meira, S. Huang, F. Yang, B. Rellinghaus, M. Chaker, D. F. Perepichka and D. Ma, Silver nanoparticle enhanced metal–organic matrix with interface-engineering for efficient photocatalytic hydrogen evolution, *Nat. Commun.*, 2023, **14**(1), 541.

93 X. Wang, L. Chen, S. Y. Chong, M. A. Little, Y. Wu, W.-H. Zhu, R. Clowes, Y. Yan, M. A. Zwijnenburg, R. S. Sprick and A. I. Cooper, Sulfone-containing covalent organic frameworks for photocatalytic hydrogen evolution from water, *Nat. Chem.*, 2018, **10**(12), 1180–1189.

94 W. Weng and J. Guo, The effect of enantioselective chiral covalent organic frameworks and cysteine sacrificial donors on photocatalytic hydrogen evolution, *Nat. Commun.*, 2022, **13**(1), 5768.

95 M. Xu, C. Lai, X. Liu, B. Li, M. Zhang, F. Xu, S. Liu, L. Li, L. Qin, H. Yi and Y. Fu, COF-confined catalysts: from nanoparticles and nanoclusters to single atoms, *J. Mater. Chem. A*, 2021, **9**(43), 24148–24174.

96 Z. Lin and J. Guo, Covalent Organic Frameworks for Photocatalytic Hydrogen Evolution: Design, Strategy, and Structure-to-Performance Relationship, *Macromol. Rapid Commun.*, 2022, 2200719.

97 Q. Yang, M. Luo, K. Liu, H. Cao and H. Yan, Covalent organic frameworks for photocatalytic applications, *Appl. Catal., B*, 2020, **276**, 119174.

98 T. He, W. Zhen, Y. Chen, Y. Guo, Z. Li, N. Huang, Z. Li, R. Liu, Y. Liu, X. Lian, C. Xue, T. C. Sum, W. Chen and D. Jiang, Integrated interfacial design of covalent organic framework photocatalysts to promote hydrogen evolution from water, *Nat. Commun.*, 2023, **14**(1), 329.

99 P. Pachfule, A. Acharjya, J. Roeser, T. Langenhahn, M. Schwarze, R. Schomäcker, A. Thomas and J. Schmidt, Diacetylene Functionalized Covalent Organic Framework (COF) for Photocatalytic Hydrogen Generation, *J. Am. Chem. Soc.*, 2018, **140**(4), 1423–1427.

100 W. Zhao, P. Yan, B. Li, M. Bahri, L. Liu, X. Zhou, R. Clowes, N. D. Browning, Y. Wu, J. W. Ward and A. I. Cooper, Accelerated Synthesis and Discovery of Covalent Organic Framework Photocatalysts for Hydrogen Peroxide Production, *J. Am. Chem. Soc.*, 2022, **144**(22), 9902–9909.

101 X. Zhang, K. Geng, D. Jiang and G. D. Scholes, Exciton Diffusion and Annihilation in an sp2 Carbon-Conjugated Covalent Organic Framework, *J. Am. Chem. Soc.*, 2022, **144**(36), 16423–16432.

102 A. C. Jakowetz, T. F. Hinrichsen, L. Ascherl, T. Sick, M. Calik, F. Auras, D. D. Medina, R. H. Friend, A. Rao and T. Bein, Excited-State Dynamics in Fully Conjugated 2D Covalent Organic Frameworks, *J. Am. Chem. Soc.*, 2019, **141**(29), 11565–11571.

103 W.-J. Ong, L.-L. Tan, Y. H. Ng, S.-T. Yong and S.-P. Chai, Graphitic Carbon Nitride (g-C3N4)-Based Photocatalysts for Artificial Photosynthesis and Environmental Remediation: Are We a Step Closer To Achieving Sustainability?, *Chem. Rev.*, 2016, **116**(12), 7159–7329.

104 G. Mamba and A. K. Mishra, Graphitic carbon nitride ($g\text{-}C_3N_4$) nanocomposites: A new and exciting generation

of visible light driven photocatalysts for environmental pollution remediation, *Appl. Catal., B*, 2016, **198**, 347–377.

105 X. Wang, S. Blechert and M. Antonietti, Polymeric Graphitic Carbon Nitride for Heterogeneous Photocatalysis, *ACS Catal.*, 2012, **2**(8), 1596–1606.

106 G. F. Liao, Y. Gong, L. Zhang, H. Y. Gao, G. J. Yang and B. Z. Fang, Semiconductor polymeric graphitic carbon nitride photocatalysts: the ''holy grail'' for the photocatalytic hydrogen evolution reaction under visible light, *Energy Environ. Sci.*, 2019, **12**(7), 2080–2147.

107 Z. Zhang, K. Leinenweber, M. Bauer, L. A. J. Garvie, P. F. McMillan and G. H. Wolf, High-Pressure Bulk Synthesis of Crystalline C6N9H3·HCl: A Novel C3N4 Graphitic Derivative, *J. Am. Chem. Soc.*, 2001, **123**(32), 7788–7796.

108 L. Lin, H. Ou, Y. Zhang and X. Wang, Tri-s-triazine-Based Crystalline Graphitic Carbon Nitrides for Highly Efficient Hydrogen Evolution Photocatalysis, *ACS Catal.*, 2016, **6**(6), 3921–3931.

109 L. Lin, Z. Yu and X. Wang, Crystalline Carbon Nitride Semiconductors for Photocatalytic Water Splitting, *Angew. Chem., Int. Ed.*, 2019, **58**(19), 6164–6175.

110 M. J. Bojdys, J.-O. Müller, M. Antonietti and A. Thomas, Ionothermal Synthesis of Crystalline, Condensed, Graphitic Carbon Nitride, *Chem. – Eur. J.*, 2008, **14**(27), 8177–8182.

111 G. Algara-Siller, N. Severin, S. Y. Chong, T. Björkman, R. G. Palgrave, A. Laybourn, M. Antonietti, Y. Z. Khimyak, A. V. Krasheninnikov, J. P. Rabe, U. Kaiser, A. I. Cooper, A. Thomas and M. J. Bojdys, Triazine-Based Graphitic Carbon Nitride: a Two-Dimensional Semiconductor, *Angew. Chem., Int. Ed.*, 2014, **53**(29), 7450–7455.

112 D. Zhao, Y. Wang, C.-L. Dong, Y.-C. Huang, J. Chen, F. Xue, S. Shen and L. Guo, Boron-doped nitrogen-deficient carbon nitride-based Z-scheme heterostructures for photocatalytic overall water splitting, *Nat. Energy*, 2021, **6**(4), 388–397.

113 Y. Wang, J. Zhang, X. Wang, M. Antonietti and H. Li, Boron- and Fluorine-Containing Mesoporous Carbon Nitride Polymers: Metal-Free Catalysts for Cyclohexane Oxidation, *Angew. Chem., Int. Ed.*, 2010, **49**(19), 3356–3359.

114 Z. Lin and X. Wang, Nanostructure Engineering and Doping of Conjugated Carbon Nitride Semiconductors for Hydrogen Photosynthesis, *Angew. Chem., Int. Ed.*, 2013, **52**(6), 1735–1738.

115 G. Dong, K. Zhao and L. Zhang, Carbon self-doping induced high electronic conductivity and photoreactivity of g-C3N4, *Chem. Commun.*, 2012, **48**(49), 6178–6180.

116 H. Yan, Soft-templating synthesis of mesoporous graphitic carbon nitride with enhanced photocatalytic H2 evolution under visible light, *Chem. Commun.*, 2012, **48**(28), 3430–3432.

117 J. Liu, W. Li, L. Duan, X. Li, L. Ji, Z. Geng, K. Huang, L. Lu, L. Zhou, Z. Liu, W. Chen, L. Liu, S. Feng, Y. Zhang and A. Graphene-like, Oxygenated Carbon Nitride Material for Improved Cycle-Life Lithium/Sulfur Batteries, *Nano Lett.*, 2015, **15**(8), 5137–5142.

118 X. She, J. Wu, J. Zhong, H. Xu, Y. Yang, R. Vajtai, J. Lou, Y. Liu, D. Du, H. Li and P. M. Ajayan, Oxygenated monolayer carbon nitride for excellent photocatalytic hydrogen evolution and external quantum efficiency, *Nano Energy*, 2016, **27**, 138–146.

119 Y. Wang, Y. Di, M. Antonietti, H. Li, X. Chen and X. Wang, Excellent Visible-Light Photocatalysis of Fluorinated Polymeric Carbon Nitride Solids, *Chem. Mater.*, 2010, **22**(18), 5119–5121.

120 T. Y. Ma, J. Ran, S. Dai, M. Jaroniec and S. Z. Qiao, Phosphorus-Doped Graphitic Carbon Nitrides Grown In Situ on Carbon-Fiber Paper: Flexible and Reversible Oxygen Electrodes, *Angew. Chem., Int. Ed.*, 2015, **54**(15), 4646–4650.

121 V. Georgakilas, J. N. Tiwari, K. C. Kemp, J. A. Perman, A. B. Bourlinos, K. S. Kim and R. Zboril, Noncovalent Functionalization of Graphene and Graphene Oxide for Energy Materials, Biosensing, Catalytic, and Biomedical Applications, *Chem. Rev.*, 2016, **116**(9), 5464–5519.

122 G. Liu, G. Zhao, W. Zhou, Y. Liu, H. Pang, H. Zhang, D. Hao, X. Meng, P. Li, T. Kako and J. Ye, In Situ Bond Modulation of Graphitic Carbon Nitride to Construct p–n Homojunctions for Enhanced Photocatalytic Hydrogen Production, *Adv. Funct. Mater.*, 2016, **26**(37), 6822–6829.

123 S. Xu, P. Zhou, Z. Zhang, C. Yang, B. Zhang, K. Deng, S. Bottle and H. Zhu, Selective Oxidation of 5-Hydroxymethylfurfural to 2,5-Furandicarboxylic Acid Using O2 and a Photocatalyst of Co-thioporphyrazine Bonded to g-C3N4, *J. Am. Chem. Soc.*, 2017, **139**(41), 14775–14782.

124 X. Chen, J. Wang, Y. Chai, Z. Zhang and Y. Zhu, Efficient Photocatalytic Overall Water Splitting Induced by the Giant Internal Electric Field of a g-C_3N_4/rGO/PDIP Z-Scheme Heterojunction, *Adv. Mater.*, 2021, **33**(7), 2007479.

125 Y. Hu, J. Wang, C. Yan and P. Cheng, The multifaceted potential applications of organic photovoltaics, *Nat. Rev. Mater.*, 2022, **7**(11), 836–838.

126 J. Li, M. Kang, Z. Zhang, X. Li, W. Xu, D. Wang, X. Gao and B. Z. Tang, Synchronously Manipulating Absorption and Extinction Coefficient of Semiconducting Polymers via Precise Dual-Acceptor Engineering for NIR-II Excited Photothermal Theranostics, *Angew. Chem., Int. Ed.*, 2023, e202301617.

127 Z. Wang, T. Hisatomi, R. Li, K. Sayama, G. Liu, K. Domen, C. Li and L. Wang, Efficiency Accreditation and Testing Protocols for Particulate Photocatalysts toward Solar Fuel Production, *Joule*, 2021, **5**(2), 344–359.

128 L. Wang, X. Zheng, L. Chen, Y. Xiong and H. Xu, van der Waals Heterostructures Comprised of Ultrathin Polymer Nanosheets for Efficient Z-Scheme Overall Water Splitting, *Angew. Chem., Int. Ed.*, 2018, **57**(13), 3454–3458.

129 T. D. Clemons and S. I. Stupp, Design of materials with supramolecular polymers, *Prog. Polym. Sci.*, 2020, **111**, 101310.

130 A. S. Weingarten, R. V. Kazantsev, L. C. Palmer, M. McClendon, A. R. Koltonow, A. P. S. Samuel, D. J. Kiebala, M. R. Wasielewski and S. I. Stupp, Self-assembling hydrogel scaffolds for photocatalytic hydrogen production, *Nat. Chem.*, 2014, **6**(11), 964–970.

131 S. Navalón, A. Dhakshinamoorthy, M. Álvaro, B. Ferrer and H. García, Metal–Organic Frameworks as Photocatalysts for Solar-Driven Overall Water Splitting, *Chem. Rev.*, 2023, **123**(1), 445–490.

132 E. Jin, S. Fu, H. Hanayama, M. A. Addicoat, W. Wei, Q. Chen, R. Graf, K. Landfester, M. Bonn, K. A. I. Zhang, H. I. Wang, K. Müllen and A. Narita, A Nanographene-Based Two-Dimensional Covalent Organic Framework as a Stable and Efficient Photocatalyst, *Angew. Chem., Int. Ed.*, 2022, **61**(5), e202114059.

133 R. Chen, J.-L. Shi, Y. Ma, G. Lin, X. Lang and C. Wang, Designed Synthesis of a 2D Porphyrin-Based sp2 Carbon-Conjugated Covalent Organic Framework for Heterogeneous Photocatalysis, *Angew. Chem., Int. Ed.*, 2019, **58**(19), 6430–6434.

134 B. Liu, H. Sun, J.-W. Lee, Z. Jiang, J. Qiao, J. Wang, J. Yang, K. Feng, Q. Liao, M. An, B. Li, D. Han, B. Xu, H. Lian, L. Niu, B. J. Kim and X. Guo, Efficient and stable organic solar cells enabled by multicomponent photoactive layer based on one-pot polymerization, *Nat. Commun.*, 2023, **14**(1), 967.

135 X. Chen, Z. Wang, J. Qi, Y. Hu, Y. Huang, S. Sun, Y. Sun, W. Gong, L. Luo, L. Zhang, H. Du, X. Hu, C. Han, J. Li, D. Ji, L. Li and W. Hu, Balancing the film strain of organic semiconductors for ultrastable organic transistors with a five-year lifetime, *Nat. Commun.*, 2022, **13**(1), 1480.